Study on the effect of coagulation tissue refinement of medical biodegradable magnesium alloys on in vivo degradation and intraosseous growth of rat femurs during long-term fixation

ラット大腿骨への長期固定において医療用生分解性マグネシウム合金の凝固組織微細化が生体内分解と骨内成長に及ぼす影響に関する研究

Ying　Zhang

Saitama Institute of Technology

February, 2023

.

Contents

Contents 1

Abstract 3

Chapter 1 Introduction 5

1.1 Biomedical Materials 6
1.2 Biomedical metallic material 7
1.2.1 Medical Stainless Steel 8
1.2.2 Medical Co-based 9
1.2.3 Medical Ti and Ti alloys 9
1.3 Biodegradable magnesium alloy 11
1.3.1 Mechanical properties 11
1.3.2 Biocompatibility 12
1.3.3 The degradation mechanism of Mg alloys in physiological environment 13
1.3.4 Advantages and disadvantages in biomedical applications 15
1.4 Modification of magnesium alloy materials 16
1.4.1 Surface modification 17
1.4.2 Alloying of bone reinforcement materials 18
1.4.3 Research status of magnesium alloys 19
1.5 The purpose of this research 19

Chapter 2 The microstructure, composition design and experiment methods of Mg-based alloy21

2.1 Preparation of Mg-based alloys with VTRC 21
2.2 Rapid solidification in producing amorphous / nanocrystalline alloys 22
2.2.1 The composition of Mg-based alloy design 22
2.2.2 VTRC production process 27
2.3 New Mg-based alloy Microstructure characteristic 29
2.4 Microstructures of magnesium alloys by different casting methods 33
2.4.1 Microstructures of magnesium alloys with different casting speeds 33
2.4.2 Rolled-Mg-RE Materials preparation 39
2.4.3 Rolled-Mg-RE Materials preparation 40
2.5 Concluding remarks 42

Chapter 3 Animal experiment design and program of Cylindrical Mg-RE alloy 44

3.1 Animals tests 44
3.1.1 Implant method 44
3.1.2 Experimental animals 45
3.1.3 Surgical procedure 46
3.2 Methods of in vivo test analysis 48
3.3 Histological observation method 49
3.5 Histological observation of visceral organs 49
3.4 Concluding remarks 50

Chapter 4 in vivo degradation and bone response in a rat femur model with long-term fixation52

4.1 Introduction 53
4.2 Materials and Methods 54
4.2.1 Materials preparation 54
4.2.2 Implant method 55
4.2.3 Micro-CT and histological assessments 55
4.2.4 In vivo degradation tests 55
4.2.5 Histological observation 56
4.2.6 Serum diagnosis 56
4.3 Results and discussion 57
4.3.1 Bone response and histological examination 57
4.3.2 In vivo degradation 59
4.3.4 Histological examination after implantation 62
4.3.5 Serum test results 64
4.4 Concluding remarks 66

Chapter 5 In vivo degradation and bone reaction of long-term fixation with twin-roll casting Mg alloy in a rat femur model 67

5.1 Introduction 68
5.2 Methods 69
5.2.1 Implant method 69
5.2.2 Micro-CT analysis 70
5.2.3 In vivo degradation tests 70
5.2.4 Histological observation 70
5.2.5 Serum diagnosis 71
5.3 Results and discussion 71
5.3.1 Bone response and histological examination 71
5.3.2 In vivo degradation 74
5.3.3 Histological examination after implantation 76
5.3.4 Serum test results 77
5.4 Concluding remarks 78

Chapter 6 Conclusions 79

References 82

Related publications 98

Acknowledgements 99

Abstract

Magnesium alloys as metal matrix biomaterials have attracted the attention of scholars. In vivo and in vivo, magnesium alloys have biocompatibility, a biodegradation process that does not produce toxic metal ions, degradation products that can be absorbed by the human body, they do not illicit a systemic inflammatory response, and they do not affect blood cells. In vivo cytological experiments have shown that magnesium alloys do not inhibit the growth and differentiation of mouse bone marrow cells, and they enhance the adhesion function of osteoblasts. The above characteristics of magnesium and its alloy make it a promising new absorbable internal fixation material with sufficient mechanical strength, non-toxicity, and no immunogenicity in vivo. Previous studies have shown that the use of the vertical twin-roll casting (VTRC) method can greatly optimize the properties of magnesium alloys, especially regarding corrosion resistance. This study investigated the influence of casting parameters on the properties of magnesium alloys.

Mg–Re alloys were prepared at different speeds such as 10 m/min, 16 m/min, 24 m/min, and 30 m/min and analyzed by electron backscattering diffraction (EBSD). The microstructure, corrosion behavior, and bone reaction in vivo were investigated in detail. The results show that the corrosion resistance of the alloy increases with an increase in the casting speed and finer grain size of the cast-rolled parts. Among the four castings, VTRC-30m/min castings had the greatest corrosion resistance. The most representative VTRC-10m/min Mg–Re alloy and VTRC-30m/min Mg–Re alloy were selected for animal experiments. The two Mg–Re alloys have also been used in previous animal studies in which the surgery was performed with healthy bones and implanted for a short period of time. Therefore, additional experimental studies are needed to determine whether Mg–Re has therapeutic effects on the clinical healing of fractures or bone injuries, and whether long-term implantation will cause damage to the body. In this experiment, two kinds of Mg–Re alloys were made into metal rods and inserted into the rat femur to simulate their effect on femoral healing under the condition of an injury, and long-term implantation was used to evaluate the effect on the body. The VTRC-30m/min implant obtained a high degree of new bone tissue in the case of a bone injury. In vivo experiments showed that the degradation performance of the VTRC-30m/min implant was better than that of the VTRC-10m/min implant, and the corrosion rate was slower and uniform in vivo. After 32 weeks of clinical implantation, the results of specimen staining, section, and serum detection showed that compared with the Control group, the liver, heart, and kidney of the rats in the VTRC-30m/min group had no pathological changes, and the cell structure was normal. The serum indexes were similar to those of the rats without Mg alloy. In conclusion, these results indicate that the casting speed has a significant effect on the tissue and degradation performance of Mg-based implants, and the degradation performance is better with an

increase in casting speed. The VTRC-30m/min Mg alloy had the least effect on the body and the best healing effect on bone injury.

To further study the effect of the casting method on the properties of the Mg alloy, Mg–A was prepared by a rolling method on the basis of the VTRC-30m/min Mg alloy with the best performance. The microstructure, degradation behavior, and bone reaction of the two alloys were studied. The microstructure analysis showed that the local orientation error of Rolled-Mg-RE was smaller than that of Mg–Re. The local orientation error in the grain leads to higher corrosion rate. Therefore, Rolled-Mg-RE has better corrosion resistance. Ti, Mg–Re, and Mg–A alloy plates were implanted into the rat femur model, and the degradation behavior was observed after 48 weeks. In vivo experiments showed no significant changes around the femur in the Ti group, excluding external factors that may lead to bone remodeling and new bone formation. Mg–A induces more new bone than Mg–Re, which is necessary to prevent pathological fracture. Staining and sectioning of the specimens showed that the liver and heart of the rats implanted with Mg alloy had no pathological changes, and the cellular structure was normal, which were similar to that of the rats without Mg alloy. Therefore, the Mg–A alloy has potential as a biodegradable implant material.

Keywords: Mg-RE alloys, microstructure, corrosion resistance, in vivo, Amorphous, Degradable, Bone response.

Chapter 1 Introduction

Bone transplantation is one of the most frequently performed tissue transplantation procedures worldwide, second only to clinical blood transfusions. Metal materials play a very important role in treating orthopedic injuries or replacing bone tissue in modern medicine. Magnesium alloys have higher mechanical strength and fracture toughness, and are more suitable for load-bearing applications. Compared with stainless steel, titanium, and cobalt-chromium alloy, Mg metal has better biocompatibility, does not produce toxic metal ions in the degradation process, can be absorbed by the human body, and does not require a second operation to remove, greatly reducing medical costs and patient pain. In addition, Mg is an essential element to maintaining daily activity, accounting for approximately 0.05% of the total body weight, more than half of which exists in the skeleton. Various in vitro and in vivo experiments have proven that Mg has good biocompatibility and biosafety. However, pure Mg corrodes too quickly under normal physiological conditions, losing mechanical integrity before bone tissue can properly heal, and producing hydrogen faster than the host tissue can process. Therefore, although magnesium as an orthopedic implant has had some success, there is still room for development.

In the past ten years, Mg alloys containing rare earth elements have attracted attention. The addition of rare earth elements such as Y, La, Ce, Nd, Sm and Gd improves the plasticity and strength of the Mg alloy, and reduces the anisotropy and tension/compression asymmetry of the magnesium alloy compared with AZ31 and other common Mg alloys. In addition to improving the ductility and strength, Mg alloys containing rare earth elements also have high creep resistance and corrosion resistance. In addition to the alloy composition, the corrosion resistance of Mg is also affected by its internal microstructure characteristics such as the grain boundary (GB), precipitated phase, grain orientation, and dislocation. Most biodegradable Mg alloys are deformed alloys, and their mechanical properties are superior to casting alloys because of the fine grain strengthening effect produced by plastic deformation.

1.1 Biomedical Materials

Biomedical materials are materials with special properties and functions, which are used for diagnosis, treatment, surgical repair, physical therapy and rehabilitation of diseases in biological systems, replacement of biological tissues or organs (artificial organs), and enhancement or restoration of their functions. And to the human body non-toxic, no side effects, no coagulation, no hemolysis, will not cause human cell mutation, change, distortion, do not cause immune rejection of the material

According to ISO 10993-1, biomedical materials are divided into three categories: surface contact devices, external access devices, and implanted devices [1]. According to the material properties, the material can be divided into five categories: biomedical metal materials, biomedical polymer materials, biomedical inorganic non-metallic materials or bioceramics, biomedical composite materials and biomedical derived materials. With the vigorous development and major breakthrough of biotechnology, biomaterials have become a hot spot in the field of R&D and have a good prospect.

Fig. 1.1 Examples of older and recent types of hip prostheses made of PMMA, stainless steel, Co- and Ti-based alloys. For each prosthesis, the year of manufacture is denoted [2].

1.2 Biomedical metallic material

At present, biomedical materials used in clinic mainly include biomedical metal materials, biomedical organic materials (mainly refers to organic polymer materials), biomedical inorganic non-metallic materials (mainly refers to bioceramics, biological glass and carbon materials) and biomedical composite materials.

Compared with several other biological materials, biomedical metal materials have high strength, good toughness and bending fatigue strength, excellent machining performance and many other medical materials can not be replaced by excellent performance.

Biomedical metal materials refer to a class of metals or alloys used as biological materials, also known as surgical metal materials. It is a class of bioinert materials. Usually used in plastic surgery, dentistry and other fields, it has the function of treating, repairing and fixing human body hard tissue system.

Among biomedical materials, metal materials have been used for hundreds of years. Humans have experimented in ancient times with the use of external materials to replace broken body tissue [3]. Since BC, humans have used natural materials, such as ivory, to repair bone tissue; In the 19th century, due to the development of metal smelting technology, people began to try to use a variety of metal materials, spare no effort to develop biomedical materials, in order to rescue patients with bone tissue defects caused by trauma, tumor, infection in clinical, such as silver amalgam (main components: mercury, silver, copper, tin, zinc) to fill teeth, etc [4].

At present, the main clinical application of medical metal materials are stainless steel, cobalt alloy, titanium and titanium alloy, etc. In addition, there are shape memory alloys, precious metals and pure metal tantalum, niobium, zirconium and so on. Table 1-1 shows the various properties of human bones and the properties of different implant materials.

Table 1-1 Properties of Human Bone and various implant materials. [6-14]

Implant Material	Density (g/cm ^{3})	Modulus of Elasticity (GPa)	Compressive Yield Strength (MPa)	Reference
Cortical/Compact bone	1.8–2.0	5–23	130–180	[5]
Cancellous/Trabecular/Spongy bone	1.0–1.4	0.01–1.57	4–12	[5] ; [6]
Magnesium	1.74–1.84	41–45	65–345	[7] ; [8]
Titanium alloys	4.4–4.5	110–117	758–1117	[9] ; [10]
Stainless steel (316 L)	7.9	190	170–310	[11] ; [6]
CoCr alloys	8.3–9.2	210–253	450–1000	[11] ; [12]
Synthetic Hydroxyapatite (HA)	3.1	73–117	600	[9]
Tri-calcium Phosphate (TCP)	3.14	24–39	2–3.5	[13]
Poly Lactic-co-Glycolic Acid (PLGA)	1.2–1.3	1.4–2.8	41.4–55.2	[13]

1.2.1 Medical Stainless Steel

Medical stainless steel is one of the earliest developed biomedical alloys. It is widely used because of its easy processing and low price. In particular, 316L stainless steel produced with the continuous improvement of modern technology was born. Its cost is low and it is mainly used as the material of joint shank and joint head. Stainless steel as a human implant has the advantages of low cost, easy processing, good strength and toughness, so it is used to make a variety of artificial joints and fracture internal fixation devices; The dental department is used for dental implant, root implant, dental orthosis, etc. The cardiovascular department is used to make cardiovascular stents, etc. In addition, medical stainless steel is also used to manufacture a variety of medical surgical instruments. but clinical results show that 316L stainless steel implanted into human body sometimes produces gap corrosion, friction corrosion, fatigue corrosion rupture and other problems under physiological conditions [15], resulting in poor long-term implantation stability. At the same time, the density and elastic modulus of stainless steel and the human body's hard tissue is relatively large, so the mechanical compatibility is poor, at the same time, stainless steel corrosion produced by nickel ions may induce the formation of tumors and no biological activity itself, other metal ions may also lead to edema, infection and tissue necrosis, difficult to form a firm combination with biological tissue. Therefore, the application of medical stainless steel is declining, but it still plays an important role in orthopedics and oral repair and replacement because of its advantages.

Fig. 1.2 Stainless steel bone reinforcement as bone fixed implants [5].

1.2.2 Medical Co-based

Cobalt - based alloy is a kind of hard alloy which can withstand various wear and corrosion and high temperature oxidation. As an artificial joint, its application began in the 1940s [16]. Due to the deficiencies in early product design and processing technology and the high friction torque and other reasons, the early clinical application effect was not ideal [17], so the research on cobalt-based alloy with wear-resistant surface has been widely paid attention to. Cobalt-based alloy has excellent mechanical properties, abrasion resistance and biocompatibility. In most cases, it remains in a passivated state in the human body, and corrosion is rare. Its abrasion resistance is also the best among all medical metals. Therefore, cobalt-based alloy is more suitable for manufacturing long-term implant parts with harsh internal load and high wear resistance requirements. Its main varieties are all kinds of artificial joints and plastic surgery implants. It has been used in cardiac surgery, dentistry and other fields. It may be that metal wear particles cause giant cells and tissue necrosis in the body, leading to joint pain and loosening. The cobalt, nickel and chromium produced by corrosion can also cause skin irritation, and its application is limited due to its high cost.

1.2.3 Medical Ti and Ti alloys

Titanium is one of the best biocompatible metals known at present, and its research in the medical field can be traced back to the early 1940s. Bothe et al. [18] and Leventhal [19]

confirmed the good biosafety of pure titanium through animal experiments, and then titanium alloy began to be applied to the medical field. However, the early titanium alloys still have defects in the aspects of biosafety, biomechanical compatibility and processing and forming, and their elastic modulus is also much different from bone tissue. Therefore, a new type of β medical titanium alloy with no toxic elements, high strength and low modulus was developed. The advantages of titanium alloy as a medical material are: light weight, density (20℃) is only 4.5g/cm^3, the human body load is light; And non-magnetic, not affected by electromagnetic fields and thunderstorms; There are no toxic side effects after implantation; At the same time, good corrosion resistance, in the immersion environment of human blood will not be easily corroded, to ensure good compatibility with human blood and cell tissue, as the implant does not produce human pollution, will not occur allergic reaction; It has high strength and good toughness. As an implant left in the human body for a long time, it has high strength and toughness when subjected to bending, torsion, extrusion, muscle contraction and other forces of the human body. Titanium alloy is used in osteosurgery to make various fracture internal fixation devices and artificial joints. It is characterized by its elastic modulus closer to that of natural bone than other metallic materials, low density and light weight. However, the wear resistance of titanium alloy is not good and there is an occlusal phenomenon. Therefore, it is necessary to pay attention to the coordination of materials in the manufacture of combined total joint with titanium alloy. In craniocerebral surgery, microporous titanium mesh can repair damaged cephalic bone and dura, and can effectively protect the cerebrospinal fluid system. Titanium alloy can also be used to make skull plates for skull reconstruction. In oral and frontal surgery, pure titanium mesh as a bone bracket has been used in the reconstruction of mandibular bone, making dentures, dentures, brackets, dental Bridges and crowns, etc. It also has good clinical effects in the fields of diurnal orthodontics and oral implantation. On the cardiovascular side, pure titanium can be used to make artificial heart valves and frames. But the wear resistance of titanium is poor, and smelting and forming processing is more difficult than other metals, so it still needs to be improved.

1.3 Biodegradable magnesium alloy

At present, materials that can be degraded and absorbed in vivo are a research hotspot of medical biomaterials. The degradable absorbent materials in clinical application are mainly polymers and some ceramic materials, such as polylactic acid and calcium phosphate, but their use is limited due to the low strength of polymer materials and the poor plastic toughness of ceramic materials. In recent years, biodegradable magnesium alloy as the main representative of the new generation of medical metal materials has attracted special attention. This kind of new medical metal material takes advantage of the harmless properties of magnesium alloy after corrosion and degradation in the human environment to realize the medical and clinical purpose of metal implant degradation in the body without causing other harm. In addition, due to the characteristics of metal materials, the plasticity, stiffness and machining properties of magnesium alloy are far superior to the existing clinical application of polylactic acid and other degradable polymer materials, so it is more suitable for clinical application in bone and other hard tissue repair.

As a biodegradable medical material, magnesium alloy is known as the third generation of biomedical materials, which has better performance compared with other materials. The elastic modulus and bone density of magnesium and its magnesium alloy are close to that of human bone, which meets the requirements of ideal bone plates. The corrosion rate is also controllable. The trace magnesium ions produced after corrosion are one of the most abundant cations in human body, and they are involved in almost all metabolic processes in human body. Therefore, it has a good application prospect in cardiovascular implantation and bone repair.

1.3.1 Mechanical properties

Magnesium alloys have good mechanical propertiesIt has higher mechanical strength than bioceramics. It is clear from Table 1-1 that because Mg's elastic modulus (E) is close to bone, it reduces the risk of stress shielding, which is outstanding in the case of permanent implants (titanium (Ti) alloy, stainless steel (SS), and cobalt-chromium (CoCr) alloy). With the presentClinical application of inert metal compared to have lower and closer toThe

elastic modulus of human cortical bone (37.5~65.0 GPa), so it canEffectively alleviates the problems of stress shielding and osteolysis [20]. Liu et al. The compressive strength of pure Mg and magnesium alloys is compared with existing commercial productsHA (Pro-Osteon ®), Ca3(PO4)2 (ChronOS®) and CaSO4(Osteoset®) and others were compared, as shown in Fig. 1.3[21]. As shown, magnesium alloyCompressive strength (260~310 MPa) and human cortical bone compressive strength(290 MPa) is very close and significantly higher than the current commercial bone repairThe compound material.

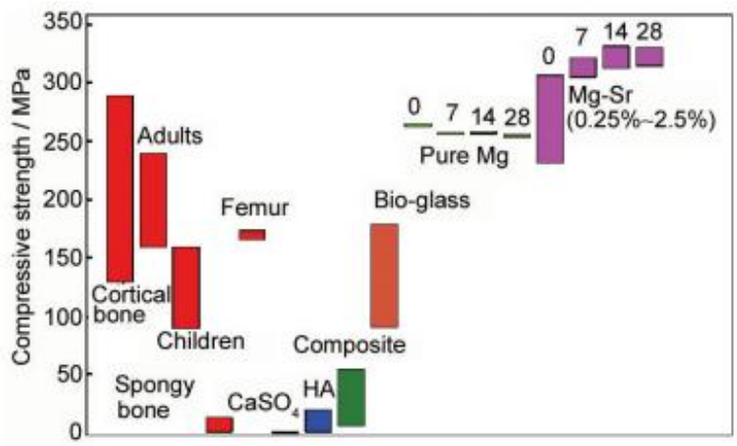

Fig. 1.3 The comparison of compressive strength for natural bone, commercial bone-grafting products and magnesium-based metals [21].

1.3.2 Biocompatibility

Mg is an essential element for human life, accounting for about 0.05% of the body's total weight, more than half of which is found in the bones. Mg^{2+} is abundant in human body, of which about 65% exist in the form of free Mg^{2+}, about 15% exist in the form of phosphate, carbonate, citrate and oxalate, and about 20% exist in the form of protein binding. Mg is involved in a series of metabolic processes in the body, and is an important part of more than 300 enzymes in the body. It is also closely related to bone, nerve, muscle and heart function [22]. In addition, Mg^{2+} in the body can regulate the structure of DNA and RNA, reduce the incidence of cancer, and enhance the antiviral ability of cardiovascular disease. It also reduces the amount of cholesterol in the blood, thereby preventing diseases such as high blood pressure, arteriosclerosis and myocardial infarction. A large number of in vitro and in vivo experiments have proved that Mg has good biocompatibility and biosafety [23-25].

1.3.3 The degradation mechanism of Mg alloys in physiological environment

Biodegradable magnesium has attracted more and more attention in recent years due to its biodegradable (absorptive) properties in human environment. Researchers have made good use of the material characteristics of magnesium (pure Mg and magnesium alloy), which is prone to corrosion (degradation) in the human environment, to realize the medical and clinical purpose of metal implants gradually degrading in the body until finally disappearing, which is expected to become a new generation of orthopedic implant materials. More than half a century ago, magnesium-based materials were found to have significant osteogenic effects, but due to the limited level of material preparation at that time, it was not further used in the clinic. In recent years, magnesium foundation materials have shown excellent comprehensive properties in orthopedic applications and come into people's attention again. The standard potential of Mg relative to the standard hydrogen electrode is -2.372 V, lower than that of other industrial alloys. It is precisely because Mg has such a low standard electrode potential that it is easy to corrode and then degrade in human environment. The oxide film is loose and porous, and can not play a good role in protecting the matrix. Especially in the corrosive medium containing chloride ions, it shows high chemical and electrochemical activity. As a degradable material, it has its natural advantages. The poor corrosion resistance of magnesium has always been considered as a shortcoming of magnesium. However, experiments show that by controlling the corrosion rate of Mg and Mg alloy, the high strength characteristics of the metal materials can be utilized to complete the implant function (such as inducing the formation of new bone tissue or supporting narrow blood vessels) in a period of time, and the diseased parts of human body can be gradually eroded and degraded by human body while repairing themselves. Finally, when the human body finishes its own repair, the allogeneic metal material completely degrades and disappears. Although its degradation mechanism is completely different from that of medical polymer materials, it can overcome the weakness of low strength of medical polymer materials and non-degradable of medical metal materials, so as to have biodegradability and high support strength characteristics.

An implant, when placed inside the human body interacts with its physiological environment. Body fluids influence the properties of Mg implants, as chemical reactions occur between them. Mg degrades rapidly in the presence of body fluids so it is important to understand the mechanism of corrosion of Mg.

Corrosion of Mg and its alloys follow an electrochemical process. In an aqueous environment i.e. in presence of body fluids following reaction occurs.

$Mg + H_2O = Mg(OH)_2 + H_2$ (1-1)

Anode reaction: $Mg \rightarrow Mg^{2+} + 2e^-$ (1-2)

Cathode reaction: $2H_2O + 2e^- \rightarrow H_2 + 2OH^-$ (1-3)

Product formation: $Mg^{2+} + 2OH^- \rightarrow Mg(OH)_2$ (1-4)

When the Mg implant comes in contact with the body fluids it gets oxidized thereby releasing Mg cations (Mg^{2+}) and electrons (Eq. (1) and Fig. 1.4a). The electrons are thus consumed for the reduction of water-producing hydroxyl ions (OH^-) (Eq. (2)). At the same time bio-molecules present in body fluids (amino acids, lipids, and proteins) also get adsorbed on the implant surface thereby affecting its corrosion. The $Mg(OH)_2$ film is formed over the surface of Mg alloy, which is insoluble and protects it from further corrosion (Eq. (3) and Fig. 1.4 b). Also, hydrogen (H_2) gas is released. As hydroxyl ions (OH^-) are generated, the pH value of the medium near the Mg surface increases making the environment alkaline. The $Mg(OH)_2$ film is stable at a high pH value (> 11.5) but at a lower pH value (< 11.5) this layer tends to cease [26]. Generally, after surgery secondary metabolic and resorptive process occurs at the implant-bone interface due to which local pH decreases. So, $Mg(OH)_2$ layer starts depleting [27]. This layer reacts with the chloride ions present in the aqueous medium (body fluids), thus forming soluble $MgCl_2$ leading to pitting corrosion on the surface (Eq. (4) and Fig. 1.4 c).

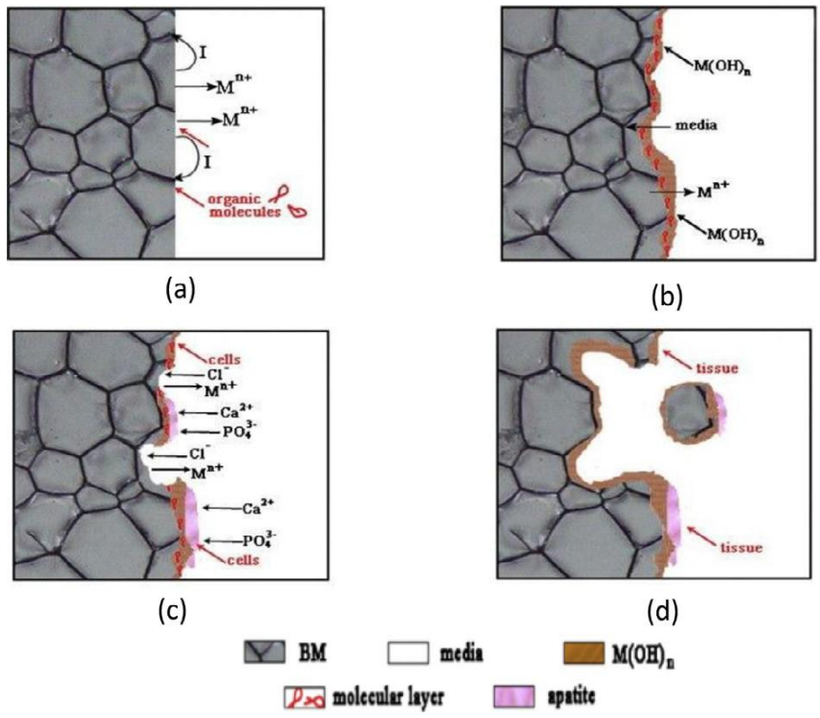

Fig. 1.4 Bio corrosion mechanism of Biodegradable metal and body fluids (M represents Mg and n = 2) [26]

The calcium and phosphate ions present in body fluids stimulate the formation of the biological apatite layer due to the alkaline environment generated (Fig. 1.4c). Since the apatite layer formed is bioactive it will allow cell adhesion and proliferation (Fig. 1.4c). The pits formed become sites for crack initiation due to stress concentration [28]. The cells thus form tissues over time. As the implantation time proceeds more degradation occurs and the corroded portion gets detached from the bulk implant (Fig. 1.4d) [29].

Due to corrosion, the mechanical integrity of the implant deteriorates. Implant corrodes away before the complete healing of bone has taken place. Also, it's evident from the reactions that hydrogen gas evolved during corrosion results in tissue separation. Keeping these key problems in mind, it is very important to control the rapid degradation rate of Mg-based implants as it causes hydrogen bubble buildup and a rise in local pH value. These changes lead to cell death and tissue inflammation.

1.3.4 Advantages and disadvantages in biomedical applications

Magnesium alloy as biomedical implant material has its unique advantages and disadvantages. Research on magnesium and its alloy in the biomedical field :(1) Magnesium is non-toxic to human body, magnesium is an essential trace element in human body, the

content of magnesium is high. Therefore, the degrading ions of magnesium do not cause any side effects; (2) The presence of magnesium ions in human bone is conducive to bone strengthening and growth; (3) Compared with other implanted metals, the density and Young's modulus of magnesium alloy are closest to that of human bone, which can reduce the interfacial stress between bone and implant materials. Mg can promote bone growth and improve implant stability. (4) Magnesium has better physical and mechanical properties than other metal bases or metals, and is more suitable for bone repair and replacement; (5) Mg has higher fracture toughness than ceramic biomaterials, higher strength than ceramic biomaterials, and more suitable elastic modulus than other commonly used degradable plastics; (6) Mg is involved in various metabolic reactions and biological mechanisms in the human body, including the formation of apatite crystals. Mg is also a cofactor and an important metal bone graft material. And stabilize the structure of DNA and RNA. (7) Magnesium ions are important from a physiological point of view, cardiovascular disease and cardiovascular disease are associated with low serum magnesium levels, and patients with peripheral artery disease are at increased risk of neuropathy.

Although magnesium alloy has the above advantages, it still has some shortcomings as a medical material. The corrosion rate cannot be controlled perfectly after implantation into human body. If the corrosion rate is too fast, excess H_2 generated in the degradation process will form air bags, which will easily cause inflammation and harm human body. Meanwhile, excessive Mg^{2+} generated at the same time will also lead to muscle paralysis, low blood pressure and respiratory diseases [30]. In addition, the disappearance of the implant before full recovery can lead to treatment failure. Therefore, controlling the corrosion rate of magnesium alloys is one of the key problems to be solved before clinical use.

1.4 Modification of magnesium alloy materials

At present, the most of researches on degradable medical Mg alloys are the commercial Mg alloys, and AZ series, such as AZ31 [31-33], AZ61 [34, 35], AZ91 [36, 37], etc. These Mg alloy materials have been applied in the industry due to their excellent performance in strength or corrosion resistance respectively. The elastic modulus of Mg alloy (45 GPa) is very close to that of natural bone (3~20 GPa) and the stress shielding

effect can be effectively avoided [38]. It has been reported that Mg can also promote osteogenesis [31]. Therefore, Mg alloys have been widely studied as orthopedic implant materials. As orthopedic materials (such as bone plate and bone screw), Mg alloy usually needs to have higher corrosion resistance to meet the performance requirements of implant material instrument.

As a bone graft material, Mg alloy has its unique advantages. However, it has been reported that Mg alloy will be seriously degraded after implantation [39,40]. How to solve the problem of too fast degradation of Mg alloy has become the focus in research. At present, the commonly used solutions are surface modification and alloying.

1.4.1 Surface modification

(1) Micro-arc oxidation (MAO) / plasma electrolytic oxidation (PEO) coating

In this coating technique, a stable oxide layer is formed on the surface of a substrate which acts as an anode connected to a cathode (usually stainless steel) in an electrolyte solution. The oxide layer thus prevents early corrosion of implant and even plays role in enhancing bioactivity.

(2) Chemical conversion coating

Conversion coatings are formed by immersing the substrate in a chemical phosphate solution for a particular time. The solution reacts with the substrate surface to form a protective phosphate conversion coating which can even stimulate bioactivity. Different phosphate solutions have been used to form different coatings. AZ31 Mg alloy coated with Ca-P coating was studied for degradation behavior in SBF for 15 days. Mass loss for coated samples was reduced by 9% that of the uncoated samples [41]

(3) Polymeric coatings

Among the polymeric coating, Polycaprolactone (PCL) is one saline solution (PSS) while the weight loss with 3% and 6% PCL was 36% and 23% respectively with a minimum rise in pH value for 6% PCL coated sample [42]. Four bio-degradable polymer coatings (PLLA, PLGA (90:10), PLGA (50:50), PCL) were used for coating Mg samples for reducing corrosion rate and a comparative study on their interaction with human endothelial cells was carried out. PLGA (50:50) coating showed better adhesion of human umbilical vein

endothelial cells (HUVEC) with a spreading morphology compared with the other three coatings. This might be because it had higher Mg^{2+} and lower Ca^{2+} concentrations in the culture medium. However, it was less effective in reducing the degradation rate of Mg than the other three [43].

(4) Bone morphogenetic proteins (BMP) coatings

Osteoinductive factors are isolated from the demineralized bone matrix, known as bone morphogenetic proteins (BMPs). Using these growth factor-based substitutes is another strategy for bone tissue engineering. BMPs display osteoinductive properties and are a part of the transforming growing factor- β superfamily. Recombinant human bone morphogenetic proteins (rh-BMP), rh-BMP2, and rh-BMP7 are the two potent growth factors that have been approved by FDA and found to be useful in a clinical setting for new bone formation [44]. AZ31B Mg alloy was coated with different concentrations of BMP2 (20, 50, 100 ng/ml), and their in-vitro cytotoxicity, in-vivo biodegradation, and bone formation were evaluated. BMP2 was coated on AZ31B alloy in combination with MAO and hydrothermal surface treatment. The in-vitro analysis concluded that BMP-2 coating increased cell proliferation as assessed by water-soluble tetrazolium salt (WST) assay and induced higher ALP activity. In-vivo the implant with 50 ng/ml BMP-2 coating showed the lowest biodegradation rate as analyzed from 3D reconstruction models of micro CT data and better bone formation as revealed by histological examination of the bone-implant interface [45].

1.4.2 Alloying of bone reinforcement materials

Alloying with suitable elements and inappropriate concentration has enabled researchers to control the corrosion rate of Mg. Properties of any material such as strength, ductility, corrosion resistance are affected by its composition. For Mg alloys, improvements in strength and corrosion resistance are linked with variations of grain size. Elements such as Aluminium (Al), Zinc, Calcium (Ca), Strontium (Sr), Yttrium (Y), Cerium (Ce), etc., are used as alloying elements in Mg-based biomaterials. Elements like Zn, Ca, Sr are present in the human body and assist in its metabolic functioning. The alloying has greatly improved the mechanical properties and corrosion resistance of purity Mg alloys. The addition of

some alloy elements can refine the microstructure. In the Mg alloy matrix, the second phase is mostly the cathode phase, and the second phase is refined after the addition of alloy elements.

1.4.3 Research status of magnesium alloys

Traditional magnesium alloys generally contain aluminum, rare earth and other elements. Currently, more researches have focused on AZ31, AZ91, WE43, etc. [27]. Wittee et al. reported earlier that four magnesium alloys, such as AZ31, AZ91, WE43 and LAE442, were implanted into the femoral bone marrow cavity of guinea pigs respectively with PLA implantation as the control. After 18 weeks, more new bone was formed around the magnesium alloy in the experimental group than in the control group, and calcium and phosphorus were deposited in the corrosion layer of magnesium alloy. The experimental results suggested that magnesium could activate osteoblasts. Promote new bone formation. Duygulu et al. [46] respectively reported that magnesium alloy AZ31 was implanted into sheep bone and rabbit bone, and both found that new bone was formed around magnesium alloy, and no influence on animal circulation, immune system and urinary system was found within a short time. Zlmng et al. [47] reported that when yttrium was added to Mg-Zn alloy with 3% zinc mass fraction, with the increase of yttrium content, the magnesium alloy grains were refined and the mechanical properties were improved. Peng et al. [48] and Hort et al. [36] studied the mechanical properties and corrosion resistance of Mg-yttrium and Mg-gadolinium dual rare earth magnesium alloys, and They believe that proper addition of rare earth elements can make magnesium alloy meet the requirements and special functions of different parts of orthopedic implants.

1.5 The purpose of this research

The content of this study is as follows.

(1) Fabrication and microstructure observation of new magnesium alloys

In the process of fracture treatment, magnesium alloy has low corrosion resistance and is prone to excessive deterioration, leading to fracture healing failure. Magnesium alloys have good corrosion resistance because magnesium ions must be released in the process of

gradual corrosion to promote bone healing. In order to solve this problem, a new casting method was used, and the influence of casting parameters on the grain refinement of magnesium alloy and the influence of grain refinement on the corrosion resistance of the alloy was further studied.

(2) Application research of new magnesium alloy materials

The alloy plate was fixed on the rat femur, and the pathological reaction of the bone tissue around the femur at different time was observed to characterize the performance of the alloy plate as a degradable fixation material.

(3) Long-term magnesium alloy implantation in rats

In order to study the effects of long-term magnesium alloy implantation on the body of the rats, the rats were dissected, the internal organs were stained, and serological diagnosis was performed.

Chapter 2 The microstructure, composition design and experiment methods of Mg-based alloy

In this chapter, the purpose of this paper is to provide a description of the experimental methods for the design and selection of magnesium based alloys used in the work of this paper.

To overcome the disadvantage of rapid degradation of biological Mg alloy, a novel Mg-based alloy with amorphous/nanocrystalline structure is designed in this chapter.

In this chapter, EDS and EBSD were used to observe the microstructure of the new materials. Evaluate the possible degradation of new materials.

On this basis, the experimental principles and methods involved in this study are described in detail, in order to understand the experimental data and conclusions of subsequent research.

2.1 Preparation of Mg-based alloys with VTRC

Metallic glass has excellent mechanical and chemical properties, which are different from solid metals, and is currently a research hotspot in the field of metallic materials [49]. In the field of biohealth, biomaterials are developing rapidly, improving people's quality of life. Among biomaterials, bioinert metals have been found to be mainly used in cardiovascular stents, orthotics and dental implants [50-51]. Among the various metallic glasses of different compositions, magnesium glass has been extensively studied in biomedicine.

A number of amorphous techniques have been developed for metallic glass, including gun and sputtering quenching [52], melt spinning [53], high pressure die casting [54-55], copper

mold casting [56] and twin-roll casting (VTRC). Compared with the traditional process, VTRC has the advantages of short production cycle, low production cost and less investment. In 1970, following Duvez's groundbreaking discovery, Chen and Miller developed a VTRC technique for producing metastable uniform flakes [57]. So far, the production technology of metallic glass strips has been almost limited to laboratory scale studies [58-64].

Previous studies have shown that VTRC is an effective technique for preparing amorphous alloy sheets with a wide range of cooling rates. Moreover, the heat transfer efficiency of vertical two-roll casting (VTRC) is higher than that of horizontal two-roll casting (HVTRC), and the cooling rate is also higher [65,66]. The rapid cooling of the alloy in the VTRC process is conducive to reducing segregation, obtaining higher uniformity, expanding solid solubility and refining microstructure characteristics [67]. It can better utilize various transition elements with limited solid solubility in magnesium alloys to improve mechanical and chemical properties [68]. As mentioned above, heat transfer VTRC is a more efficient continuous production method for magnesium alloy sheet than HVTRC, which can achieve a wide range of variable casting speed [69], thus improving the machining performance and application performance of the product.

2.2 Rapid solidification in producing amorphous / nanocrystalline alloys

2.2.1 The composition of Mg-based alloy design

The amorphous/ nanocrystalline alloys are characterised by an amorphous structure, from which interesting properties stem. However, their stability is moderate so that they can loose all their peculiar properties when annealed. By rapid solidification glasses can be

produced in different forms (powders by gas atomisation, ribbons by means of planar flow casting, wires, surface layers and others). The range of applications and the industrial interest for amorphous alloys have been continuously growing during the last years and various materials are commercially available nowadays [70]. The major field of applications is related to the peculiar magnetic properties of Fe, Ni and Co based amorphous alloys, which represent a valid alternative to the traditional soft magnetic materials. The composition ranges of alloys that can be quenched to the glassy state depend on the production technique. Increasing the cooling rate enhances the glass forming range for a given system. The types of alloys showing good glass forming ability are summarized in Table 2-1.

In order to retain an expect structure from the melt, (1) appropriate quenching techniques must be applied, and (2) careful alloy selection must be made. Considering from the topological aspect, atomic radii of candidate alloying elements for magnesium alloys are listed in Table 2-2. Atomic size differences between the alloying elements and magnesium (aluminum) are also calculated which symbolized by ASD_{Mg} (ASD_{Al}).

Table 2-1 A selection of glass-forming alloy systems

Main components	Minor components	Examples
Late transition metal Fe, Co, Ni	Metalloid B, P, Si	Fe-B, Fe-Ni-B Fe-B-Si, Co-Fe-B-Si
Early transition metal Ti	Metalloid Si	Ti-Si
Early transition metal Nb, Zr, Ti	Late transition metal Ni,Cu	Cu-Zr, Cu-Ti Ni-Zr, Ni-Ti

Aluminium	Rare earth-Late transition metal:	Al-La, Al-Sm, Al-Ce
Al	La, Ce, Sm, Ni, Fe	Al-Ni-Y, Al-Fe-Ce
Rare earth	Late transition metal	La-Au, Gd-Co, Gd-Fe
La, Gd	Fe, Ni, Co	La-Al-Ni
Alkaline earth	Metal	Mg-Cu-Y
Mg, Ca	Al, Cu, Y	Ca-Al

The AZ series magnesium alloy is a kind of commonly used commercial magnesium alloy. The alloy composition design considers Mg and Al as the main elements of the Mgbased alloy. According to the Inoue radius principle and Table 2-2, it can be seen that the selected elements mainly include Ca, Ge, La, Ce, Si, Ni, Sm and Gd. According to Table 2-1, the Aluminum - Rare earth – Late transition glass-forming alloy system has the most combinations of these elements. It is well kown that the rare earth (RE) element has a characteristic of so-called—scavenger effect in Mg-based alloys, and impurity elements can form less cathode intermetallic compounds with rare earth elements. In addition, it has been reported that rare-earth elements (La, Ce) can improve the corrosion resistance of Mg alloy materials [71]. Considering the above analysis, we adopted La and Ce elements in the composition design scheme.

Table 2-2 Atomic radius of some common elements used in Mg alloys

Elements	Radius / nm	ASD_{Mg} / %	ASD_{Al} / %
Mg	0.160	-	11.85
Zn	0.139	12.92	2.60
Ca	0.198	23.40	38.02
Ge	0.124	22.56	13.39
Cu	0.128	20.19	10.74
Mn	0.135	15.69	5.71
Al	0.143	10.59	-
Ti	0.146	8.73	2.08
Ce	0.183	13.95	27.45
La	0.188	17.34	31.24
Si	0.115	27.30	19.47
Y	0.180	12.50	25.82
Fe	0.127	20.63	11.90
Ni	0.124	22.50	13.29
Zr	0.160	0.08	11.90
B	0.095	40.63	33.57
Co	0.126	21.25	11.89
Sm	0.180	12.50	25.87
Gd	0.180	12.50	15.87

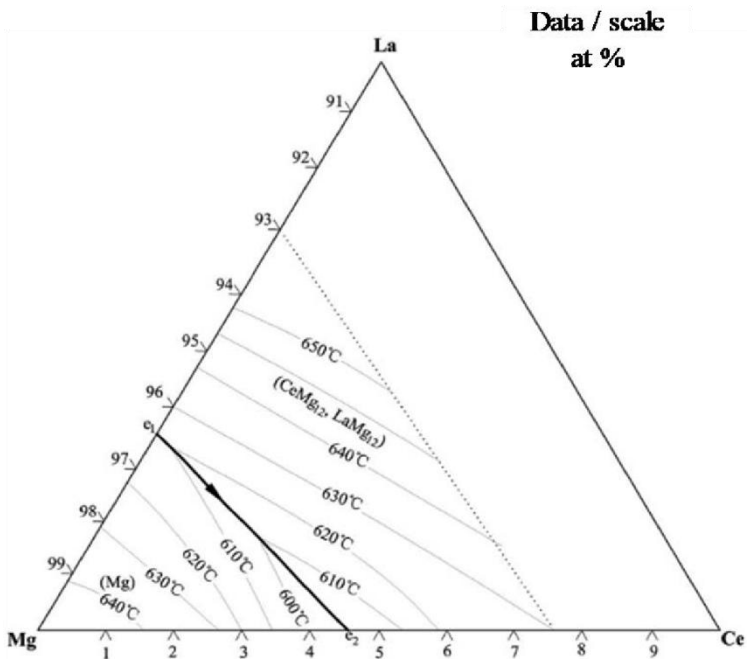

Fig. 2.3 Projection of Mg- rich angle on liquid surface of ternary phase diagram of Mg-Ce-La [72].

Through the above analysis, the Ce and La were added to the Mg-based alloy in this research, and their ternary phase diagram with magnesium (Mg-Ce-La) is shown Fig. 2.1 [73]. According to the ternary phase diagram, it is feasible to prepare the new Mg-RE (rareearth) alloy by VTRC process under the current casting conditions with the addition of rareearth elements (Ce, La).

Table 2-3 Composition and the atomic radius of the Mg-RE alloy (atomic radius difference between Mg (Al) and other elements is symbolized by ARD_{Mg} (ARD_{Al}).

Elements	Mg	Al	Si	Mn	Cu	Fe	Zn	La	Ce
at%	95.253	3.460	0.145	0.132	0.040	0.041	0.053	0.297	0.579
wt%	90.770	3.660	0.160	0.284	0.101	0.090	0.136	1.618	3.181
Radius/nm	0.160	0.143	0.134	0.132	0.128	0.126	0.139	0.187	0.182
ARD_{Mg}/%	-	10.63	16.25	17.50	20.00	21.25	13.13	16.87	13.75
ARD_{Al}/%	11.88	-	6.29	7.69	10.50	11.88	2.78	30.77	27.27

Ingots of Mg-RE alloy were prepared by induction melting the mixture of industrial AZ31, Mg-10%La and Mg-20%Ce (wt%) master alloys in an induction furnace at 993 K

for 30 min under the protection of high-purity argon. The chemical compositions of the ingots were measured by X-ray fluorescence spectrometry, and the results are listed in Table 2-3

2.2.2 VTRC production process

All materials in the studies were fabricated with vertical-type twin roll casting (VTRC) system. The VTRC experiments were carried out on a vertical-type twin roll casting mill with two identical rolls made of copper alloy. The diameter and width of both rolls are 300 mm and 100 mm respectively. In consideration of the separation force generated in the casting process, metal blocks were set at the two rotating rolls side to form a supporting force, minimizing the roll gap during casting process as much as possible. When the alloy melted completely, the melt was introduced into the roll gap between the left and right rolls through the asbestos casting nozzle, Twin roll casting experiments were carried out under casting conditions with a casting speed of 30 m/min and a pouring temperature 973 K. Because the casting produces separation force during the casting process, the metal block was set at the side of the moving roller to form a supporting force in order to minimize the gap between the rollers as much as possible during the casting process. Afterward, the melt of magnesium alloy flowed through a nozzle to a position between running rolls. The initial roll gap was set to 0 mm. An oil tank was set under the roll and the Mg-RE alloy sheet was completely submerged in the tank when the casting process was completed to prevent further grain growth. The final thickness of the sheets between 0.5 mm and 1.1 mm and the width of the strip rang is 25 mm to 50 mm. The schematic diagram and practicality illustration of VTRC are shown in Fig. 1.5a and Fig. 1.5b, respectively.

High purity of Mg ingot (99.99%), AZ31 ingot, Mg-10La and Mg-20Ce (in wt.%) were used as raw materials. The melting process was carried out in a resistance furnace under the protection of shielding gas ($SF_6$10% and CO_2 90%). AZ31 sheets in this study were produced by melting Mg ingot and AZ31 ingot. The Mg-RE sheets in this study were produced by melting Mg ingot, AZ31 ingot, Mg-10La and Mg-20Ce.

Previous studies have shown that Mg-RE alloy plates prepared by vertical two-roll continuous casting machine have crystal phases containing amorphous phases [74].

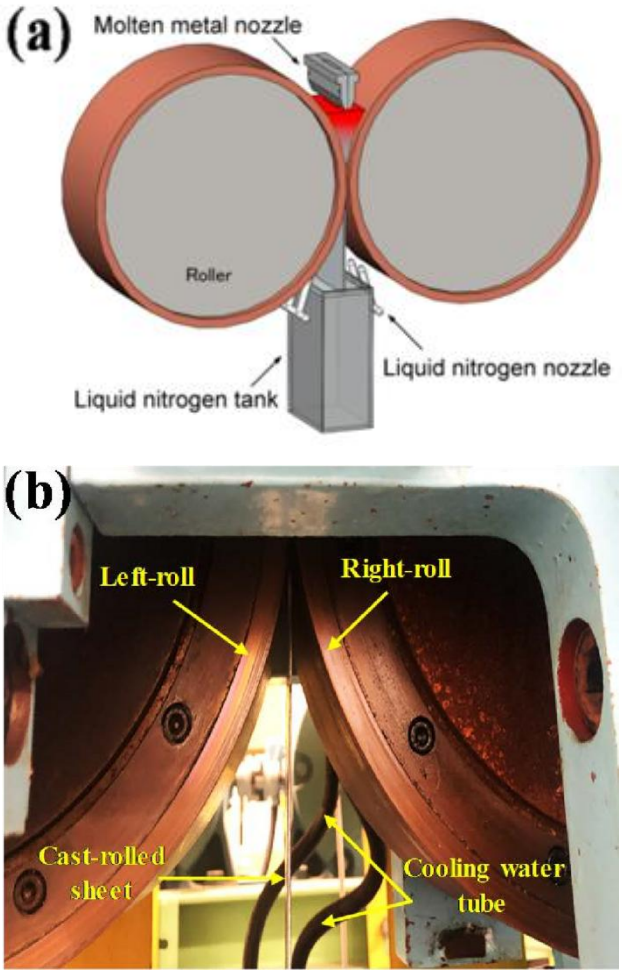

Fig. 2.2 Schematic diagram (a) and practicality illustration (b) of VTRC technique.

2.3 New Mg-based alloy Microstructure characteristic

From the Mg-RE master ingots and the as-extruded Mg-RE sheets, samples with a dimension of 10 × 10 × 1 mm^3 were firstly grounded with SiC papers to1200 grid, and then by diamond pastes down to #0.25 μm grade. The microstructures of the polished surfaces were observed using a field emission scanning electron microscope (FE-SEM, JMS-6301, Tokyo, Japan) and the elements distribution maps were observed by electron probe micro-analysis (EPMA, JXA-8530F, Tokyo, Japan). The alloy phases were obtained by an X-ray diffractometer (XRD, D/Max 2500 PC, Tokyo, Japan).

Fig. 2.3 reveals the surface morphologies and EDS analyses of the as-cast Mg-RE alloy ingot. It can be seen from Fig. 2.3 (a) that acicular intermetallic compounds crystallize in the Mg-RE alloy ingots. Fig. 2.3 (b) presents the combined EDS results, and the acicular compound crystallization in the red rectangle contains higher contents of Ce elements. Fig. 2.4 (a) presents the microstructure of the Mg-RE alloy sheet at a thickness of ~1.1 mm and a width of ~50 mm obtained at the casting speed of 30 m/min, in which the microstructure of the Mg-RE alloy sheet is characterized by dendrites of fine grains and a closely spaced secondary dendrite axis. Apart from that, as shown by the red rectangular area in Fig. 2.4 (a), it can be seen that there are portions where no appreciable crystalline features can be observed. Fig. 2.4 (c) shows the XRD patterns of the studied alloys. It can be concluded that the as-cast Mg-RE alloy sheets (Fig. 2.4a) consisted mainly of α-Mg, La-Al and Ce-Al, and it is worth noting that a broad peak appears at the angle of 20°~30°, indicating that the sample may contain both crystalline and amorphous phases.

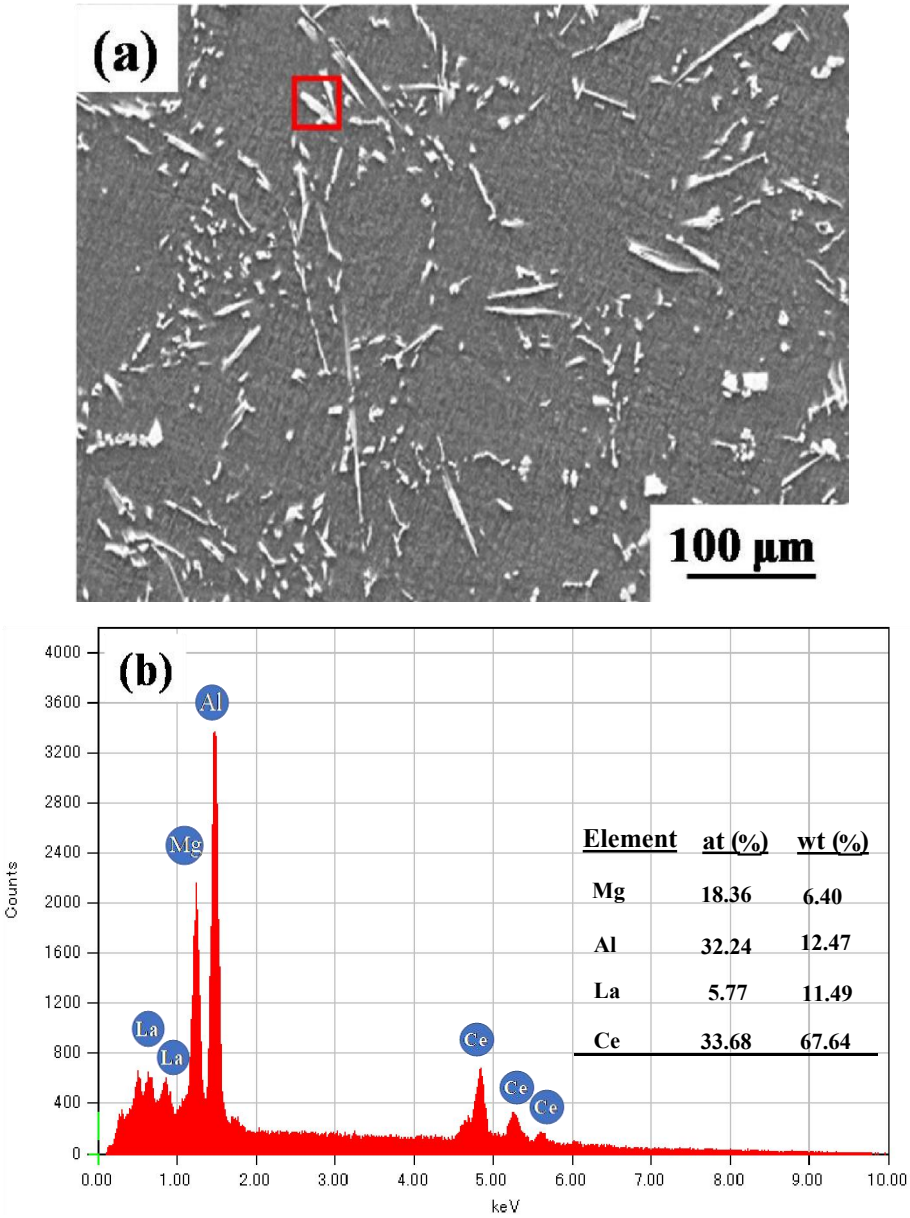

Fig. 2.3 The SEM morphologies (a) and the precipitation by EDS analysis (b) of as-cast Mg-RE alloy ingot.

The crystallite size of each detected phase in Fig. 2.4 (c) could be calculated using the Scherrer equation, which is expressed by $D_{hkl} = K\lambda/B_{hkl}\cos\theta$ [75], where D_{hkl} is the grain size perpendicular to the lattice planes, *hkl* are the Miller index of the planes being analyzed, *K* is a constant numerical factor called the crystalliteshape factor, λ is the wavelengths of the X-rays, B_{hkl} is the width of the X-ray diffraction peak in radians and θ is the Bragg angle. The

calculated results are listed in Table 2-3. It turns out that the grain sizes of the detected phase are very fine. However, the X-ray tube on the line focus side is unsuitable for analyzing such a specific area without crystals, as the line focus range is 0.1~0.2 mm wide and 8~12 mm long [76]

To solve these problems, the structure of the areas without crystals was analyzed by means of micro area X-ray diffraction. In the current operation, a collimator that was 0.03 mm in diameter was situated at the point focus side of the X-ray tube. Therefore, very small specific areas could be analyzed without reflecting unnecessary regional structural information. Fig. 2.4 (d) displays the μXRD of the areas without crystals of the Mg-RE sheet. The amorphous structure was determined by a peak that does not correspond to any sharp crystalline peak. As shown in Fig. 2.4 (b) and Table 2-4, very fine grains and dendrites with closely spaced secondary dendrite axes can be found around a large amorphous region.

Fig. 2.5 presents the values of enthalpy of mixing ($\Delta Hmix\ [AB]$) calculated by Miedma's model for atomic pairs between major elements of Mg-RE sheet samples, in which the enthalpy of mixing between Rolled-Mg-REl, Mg-La and Mg-Ce are −2 KJ/mol, −7 KJ/mol and −7 KJ/mol, respectively, while the enthalpy of mixing between AlLa and Al-Ce are −38 KJ/mol, which is greater than that between Mg and other major elements [77]. The design of Mg-RE alloy conforms to the three rules summarized by Inoue et al. [78] for the glass forming ability (GFA) of alloys: first, a multi-component system consisting of more than three major elements; second, the difference in atomic size between major elements is large (greater than 10%), and in line with the relationship of large, medium and small; third,

the mixed heat between the main elements is a suitable negative value. In other words, Mg-RE alloy has good glass-forming ability.

Table 2-4 Crystallite sizes of the Mg-RE alloy sheet, calculated by Scherrer equation

(hkl)	(100)	(002)	(101)	(102)	(110)	(103)
D_{hkl}/nm	5.1	14.2	7.8	10.6	16.6	17.9

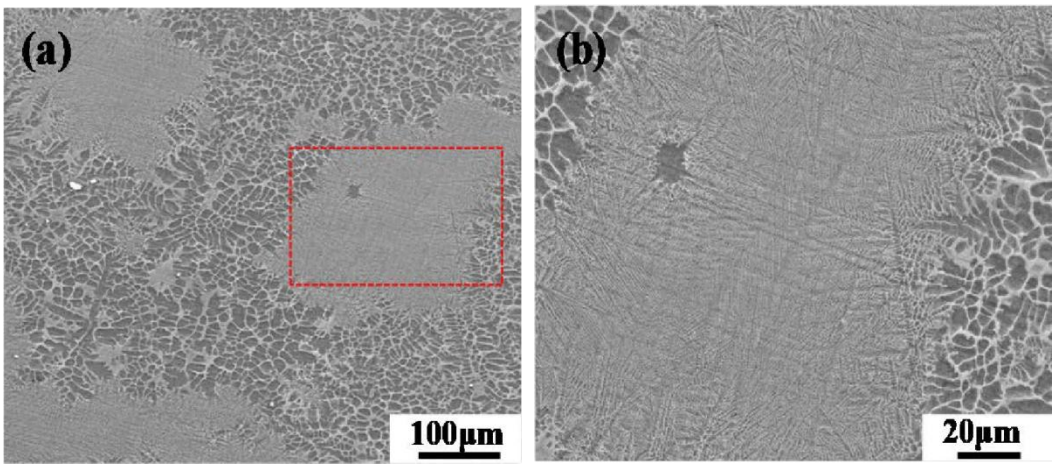

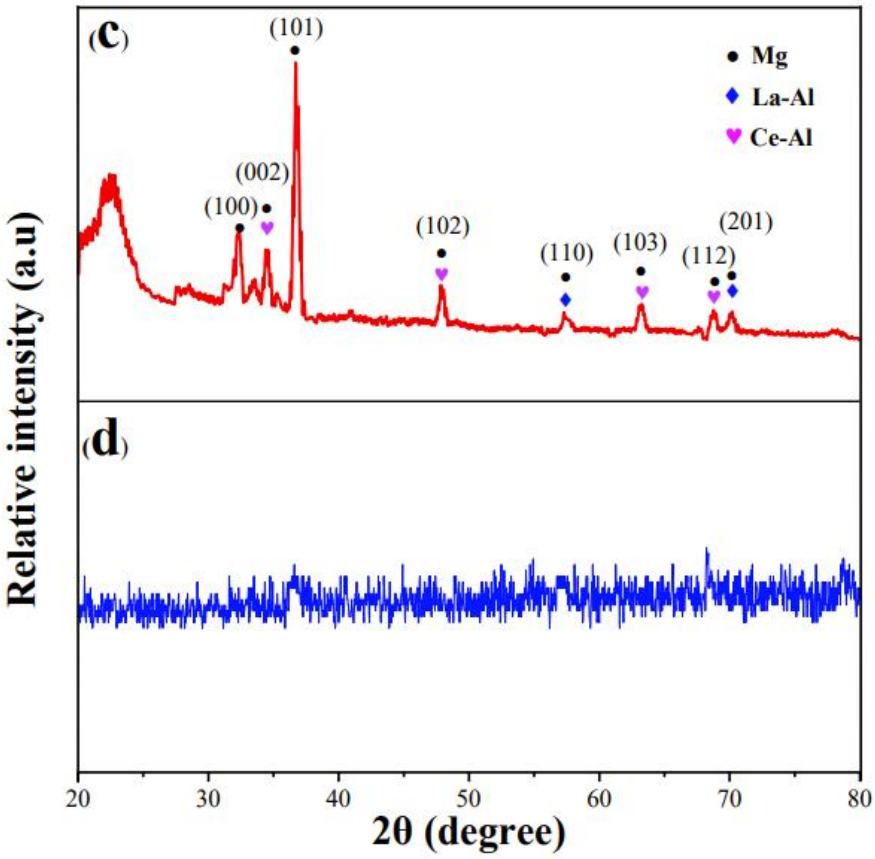

Fig. 2.4 The SEM micrographs and X-ray diffractometry (XRD) patterns of as-cast Mg-RE sheet: (**a,c**) SEM micrographs and XRD of the Mg-RE sheets. (**b**,**d**) SEM micrograph and μXRD of local amorphous region.

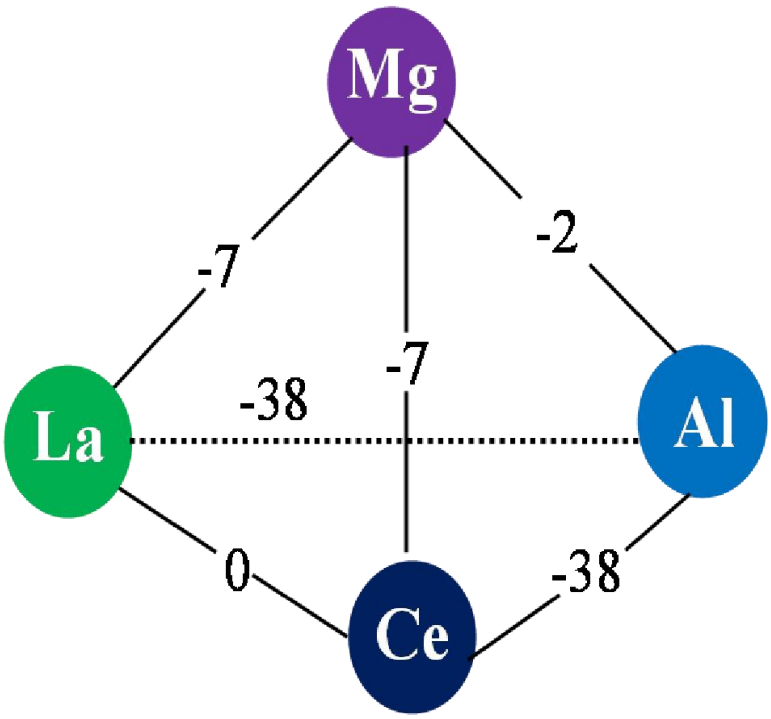

Fig. 2.5 The values of ΔH_{mix} *[AB]* (KJ/mol) calculated by Miedma's model for atomic pairs between major elements of Mg-RE sheet samples.

2.4 Microstructures of magnesium alloys by different casting methods

2.4.1 Microstructures of magnesium alloys with different casting speeds

EDS in Mg-RE alloy of VTRC-10m/min, VTRC-16m/min, VTRC-24m/min and VTRC-30m/min samples are shown in Fig. 2.6a, 2.6b, 2.6c and 2.6d, respectively. Fig. 2.6 shows the solute element distribution of Mg-RE with VTRC. It can be seen that Mg elements are evenly distributed along the matrix, while Al/Ce/La are concentrated in amorphous areas. In addition, Al, Ce, La element segregation exists between crystal phase and the amorphous region. Meanwhile,

the grain boundary is prone to segregation, because the relative atomic radius difference (ARD_{Mg}) between Mg and other elements is more than 10%, as shown in Table 2-5. It can also be found that Al, Ce and La elements are enriched in the amorphous phase region, which may be related to the fact that the alloy is prone to producing very stable Al-RE compounds under the solidification condition of low cooling rate.

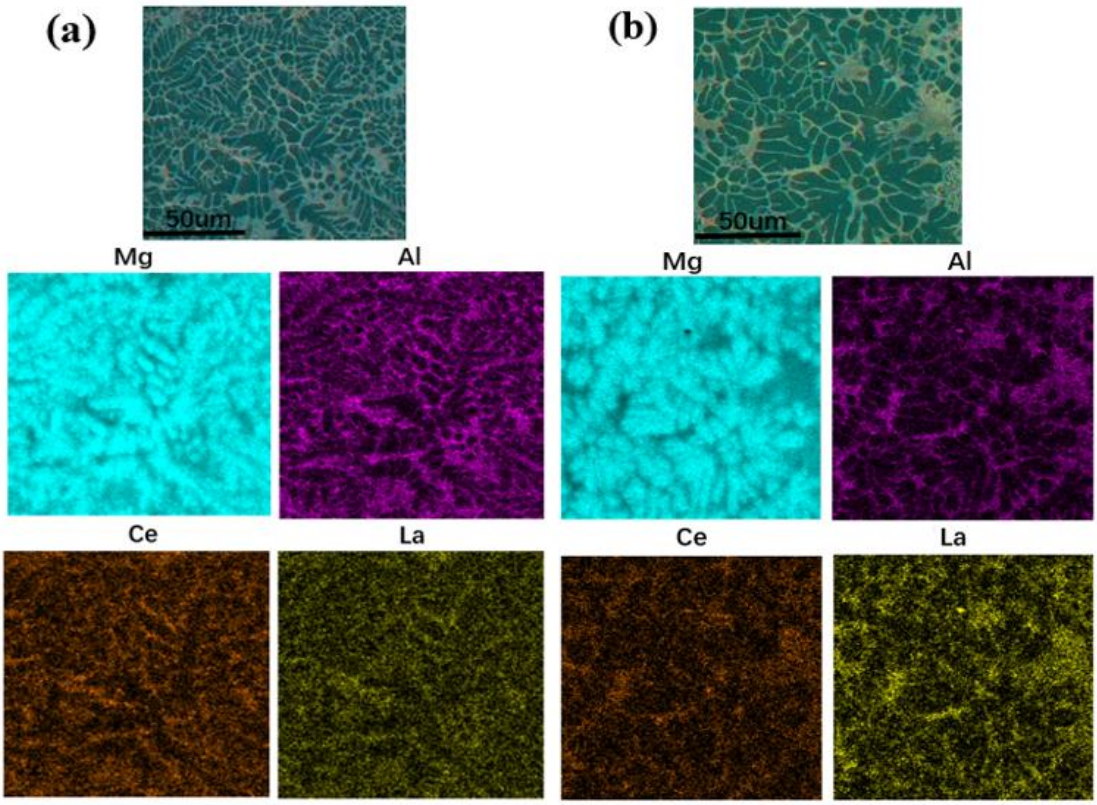

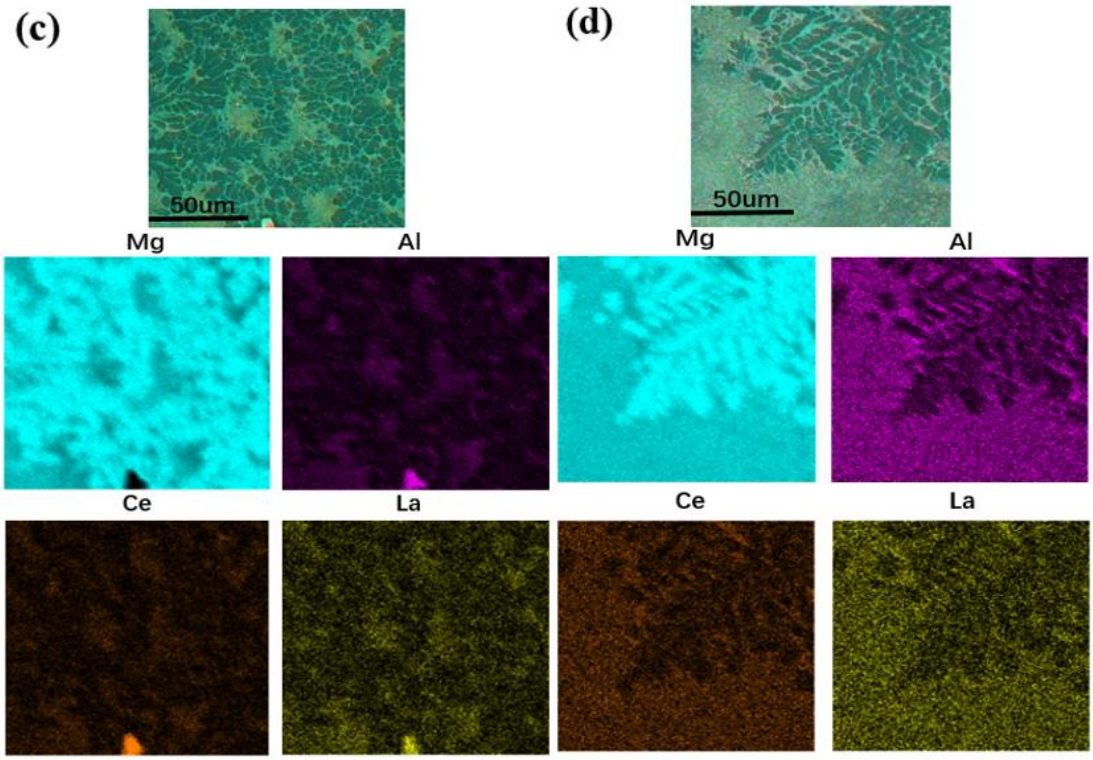

Fig. 2.6. Microstructures and EDS of the Mg-RE alloys under different conditions: (a) VTRC-10 m/min; (b)VTRC-16 m/min; (c) VTRC-24m/min; (d) VTRC-30 m/min

Table 2-5 Composition and the atomic radius of the Mg-RE alloy (atomic radius difference between Mg (Al) and other elements is symbolized by ARD_{Mg} (ARD_{Al})

Elements	Mg	Al	Si	Mn	Cu	Fe	Zn	La	Ce
at% wt%	95.253	3.460	0.145	0.132	0.040	0.041	0.053	0.297	0.579
	90.770	3.660	0.160	0.284	0.101	0.090	0.136	1.618	3.181
Radius/nm	0.160	0.143	0.134	0.132	0.128	0.126	0.139	0.187	0.182
ARD_{Mg}/%	-	10.63	16.25	17.50	20.00	21.25	13.13	16.87	13.75
ARD_{Al}/%	11.88	-	6.29	7.69	10.50	11.88	2.78	30.77	27.27

The cross-section microstructure of the polished surface was observed by scanning electron microscope (SEM) with energy dispersive spectroscope (EDS) (SEM, JXA-8530F, Tokyo, Japan), and the electron backscatter diffraction (EBSD) electron microscopy (SEM, Gemini300, Germany & EBSD, OXFORD C-Nano, England) was

used to characterize the sample microstructure including GB, grain orientation, texture, and residual strain. Channel 5 analysis software was used to analyze the EBSD results. EBSD measurement samples were prepared by conventional grinding and diamond polishing (0.5 μm), and Ar^+ ion milling was performed in a precision ion polishing system (M4000PLUS). Imaging was performed under a liquid nitrogen cooling system at an operating acceleration voltage of 3 kV and incident angle of 40°.

EBSD method was used to study the microstructure evolution of VTRC-10m/min, VTRC-16m/min, VTRC-24m/min and VTRC-30m/min magnesium alloys in RD, TD and ND directions, RD, TD and ND are respectively the rolling, Horizontal and normal directions of the microstructure. Fig. 2.7 shows the reverse pole map (IPF) plots for RD, TD, and ND samples. The IPF diagram shows the Mg alloy prepared by VTRC and the microstructure from the direction along RD, TD, and ND, as shown in Figure. The compression direction RD is the rolling direction. The compression direction TD is horizontal. The compression direction ND is the rolling direction. The colors in the figure indicate the orientation of the compression axis with respect to the local lattice according to the IPF triangle. It can be seen from the figure, with the change of casting speed, there is no significant difference in the orientation of Mg alloy grains in each direction.

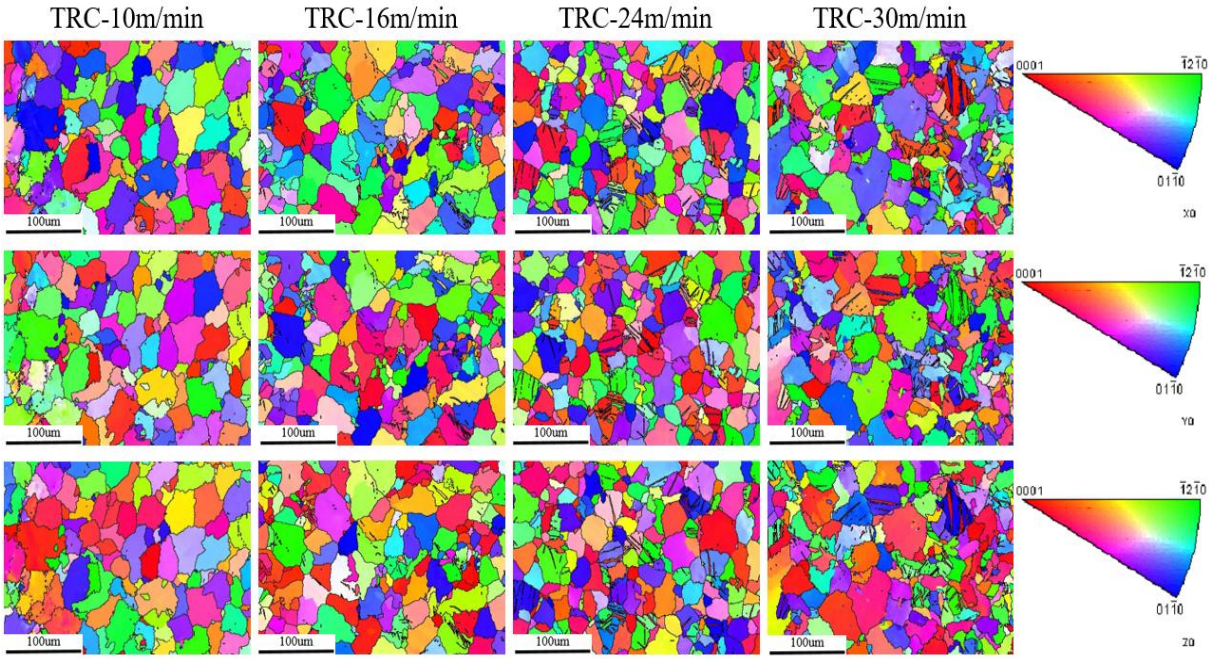

Fig. 2.7. EBSD micrographs of the four magnesium alloys.

As shown in Fig. 2.8a ~ 2.8d, the average grain size of the alloy decreased from 29.2um to 25.5um with the increase of casting speed, and as shown in Fig. 2.8e ~ 2.8h, the low-angle grain boundary (LAGB) decreased from 53.8% to 38.3% with the increase of casting speed. Previous studies showed that, Local orientation errors in the grain lead to higher corrosion rates. The larger the LAGB value, the larger the local orientation error. In the absence of local orientation error, grain orientation has limited influence on corrosion rate [79]. It can be concluded that the GB orientation deviation of Mg alloy decreases with the increase of casting speed. Therefore, VTRC-10m/min alloy has the highest corrosion rate and VTRC-30m/min alloy has the lowest corrosion rate among the four magnesium alloys.

A distinct feature of the VTRC process is the large thermal gradients along the thickness leading to rapid directional solidification [74]. Therefore, combined with the rolling effect, cellular mechanism, dense secondary dendrites, amorphous and fine grains are the common crystallization characteristics of as-cast VTRC sheets. In the process of casting

and rolling, the cooling intensity of the casting and rolling zone mainly depends on the distance of casting and casting speed. In this study, the receding distance hardly changed during the casting process. In the case of 30m/min, the contact time between the metal melt and the roller shell is nearly three times that of the case of 10m/min. Therefore, the cooling intensity of the former is three times higher than that of the latter.

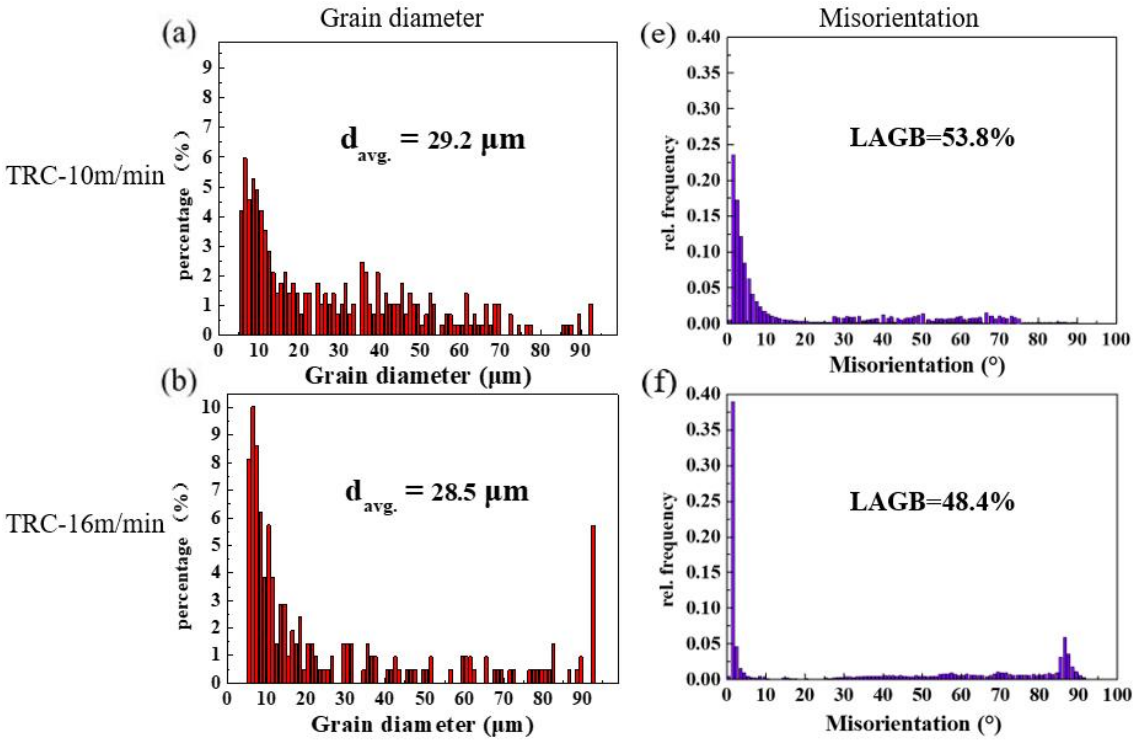

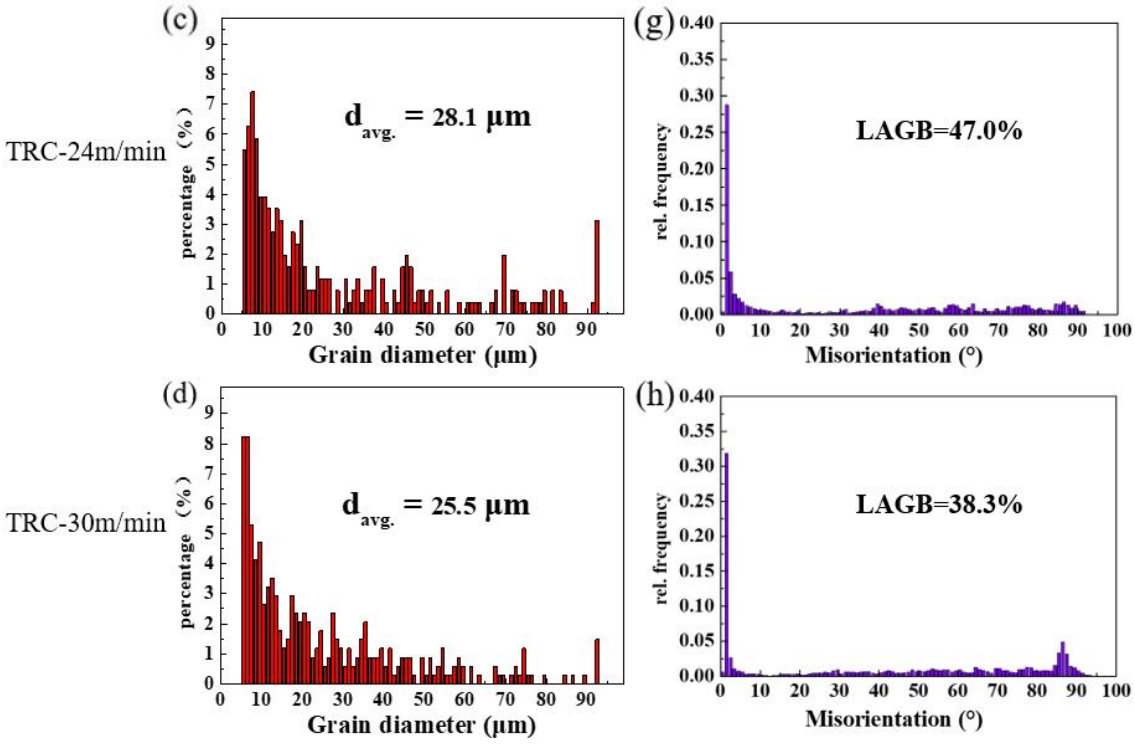

Fig. 2.8. (a-d) Grain size distribution and (e-h) grain boundary orientation deviation.

According to the basic principle of solidification, constitutive supercooling will be formed at the solid-liquid interface. The solid-liquid interface repels the solution and accumulates solutes, so that the cell structure can grow stably under the initial small disturbance. As the cooling rate increases, the secondary dendrites form dense secondary dendrites instead of cellular mechanisms. In this study, the alloy was extruded and deformed, which means that grain growth and recrystallization occur during solidification. When the cooling rate is high, complete recrystallization will not occur due to the change of crystal structure. EBSD results show that the higher the casting speed, the lower the recrystallization rate of Mg-RE alloy. The experimental results agree well with the theory.

2.4.2 Rolled-Mg-RE Materials preparation

In this experiment, high purity Mg ingot (99.99%), AZ31 ingot, Mg-10LA ingot, and Mg-20Ce ingot (wt.%) were used as raw materials. Smelting occurred in a resistance furnace

protected by high purity argon gas. The AZ31 sheet was prepared by Mg ingot and AZ31 ingot smelting, and the Mg-RE sheet was prepared by Mg ingot, AZ31 ingot, Mg-10La, and Mg-20Ce smelting. First, the Mg ingot and AZ31 ingot were placed in the resistance furnace and heated to 720°C for 1.5 h to completely melt the compound. Mg-10La and Mg-20Ce ingots were then added to the melt and the temperature was reduced to 700°C and held for 1.5 h, producing the Mg-RE alloy. A rectangular 50 × 100 × 10 mm^3 Mg-RE alloy ingot plate was hot rolled at 250°C, reducing the total thickness of the composite sample by 88.0% to produce the Rolled-Mg-RE sample.

As shown in Fig. 3.6, the I process uses VTRC technology to cast Mg-RE (Ce, La) alloy, and the II process uses additional 250°C hot rolling to produce another Mg alloy, Rolled-Mg-RE.

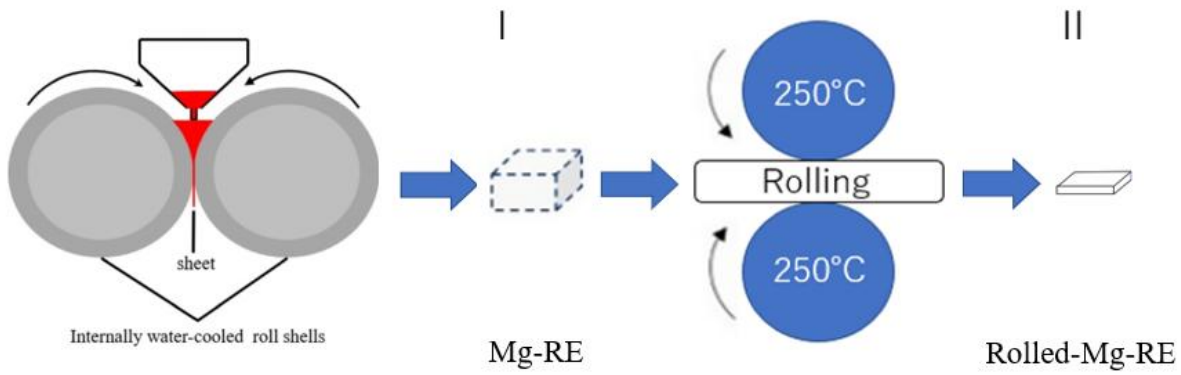

Fig. 2.9. Schematic diagram of the magnesium alloy sheet manufacturing process. A new Mg-rare earth alloy (Ce, La) was prepared by vertical twin-roll casting (VTRC) and additional rolling to obtain another Rolled-Mg-RE alloy.

2.4.3 Rolled-Mg-RE Materials preparation

The microstructure evolution of Mg-RE and Rolled-Mg-RE magnesium alloys along RD, TD, and ND directions was studied using EBSD. Fig. 2.7 shows the inverse pole figure (IPF) diagrams of the RD, TD, and ND samples. The IPF figure shows the microstructures of the Mg-RE alloy prepared by VTRC and the Rolled-Mg-RE alloy hot rolled from Mg-RE along

the RD to the true strain level shown in the figure. The compression direction RD is the rolling direction. The compression direction TD is the horizontal direction. The compression direction ND is the rolling direction. The colors in the figure indicate the direction of the compression axis relative to the local lattice frame according to the IPF triangle. Compared with Mg-RE, Rolled-Mg-RE showed extrusion deformation during the manufacturing process and grain growth and recrystallization during solidification.

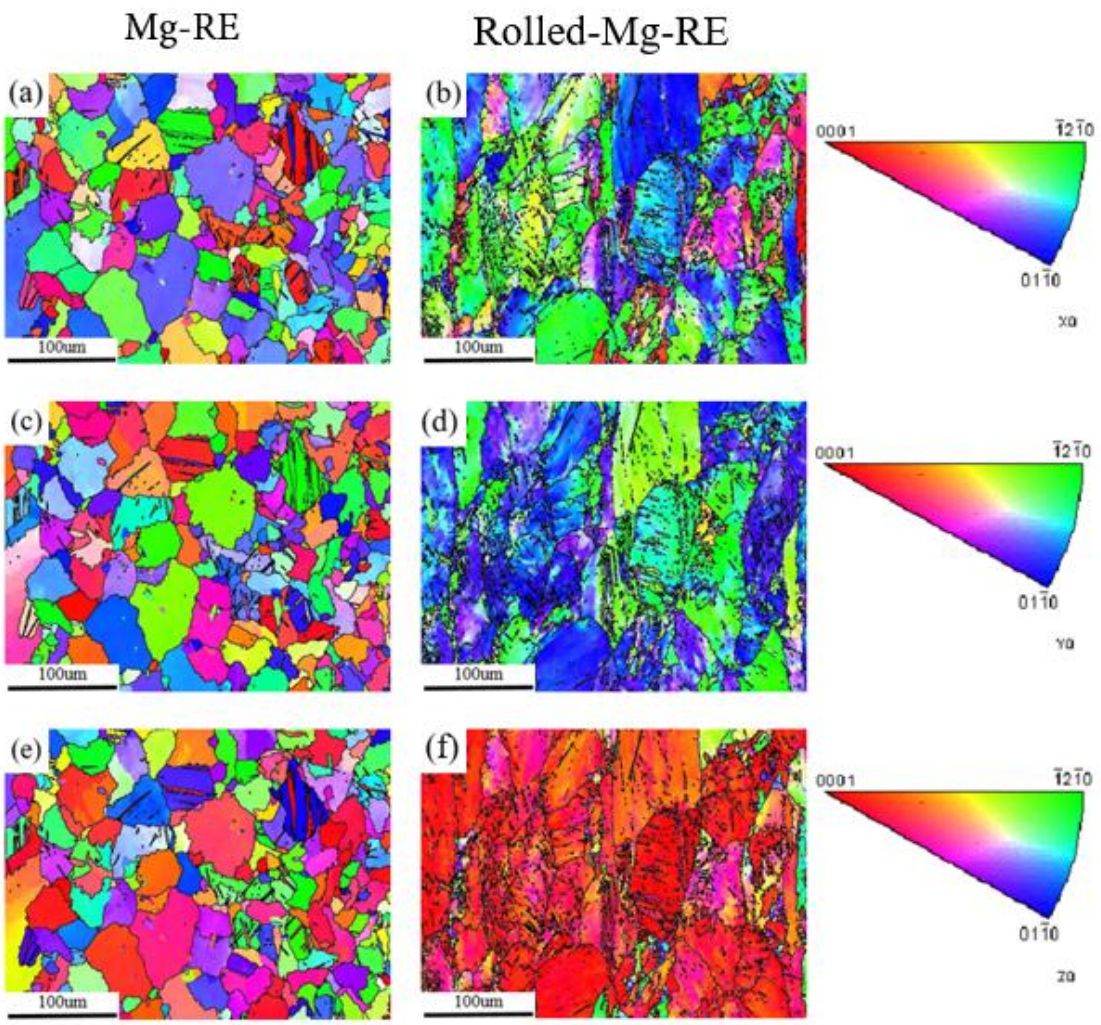

Fig. 2.10. EBSD micrographs of (a)(c)(e) an unrolled magnesium alloy Mg-RE and (b)(d)(f) hot rolled magnesium alloy Rolled-Mg-RE.

As shown in Fig. 2.8a and 4b, the low-angle grain boundaries (LAGB) of Mg-RE and Rolled-Mg-RE are 38.3% and 35.8%, respectively. Fig. 4.4c shows that the average particle size of Mg-RE was 25.5 μm. Rolled-Mg-RE shows dynamic recrystallization after hot rolling

at 250°C; however, the grain size was not uniform. As shown in Fig. 2.8d, the average particle size decreases rapidly to about 11.7 μm. Previous studies have shown that local orientation errors within grains lead to higher corrosion rates. The larger the LAGB value is, the larger the local orientation error is. In the absence of local orientation error, grain orientation has limited influence on the corrosion rate [76]. After hot rolling at 250°C, the GB orientation deviation of Rolled-Mg-RE is less than that of Mg-RE; therefore, the corrosion rate of Rolled-Mg-RE is less than that of Mg-RE.

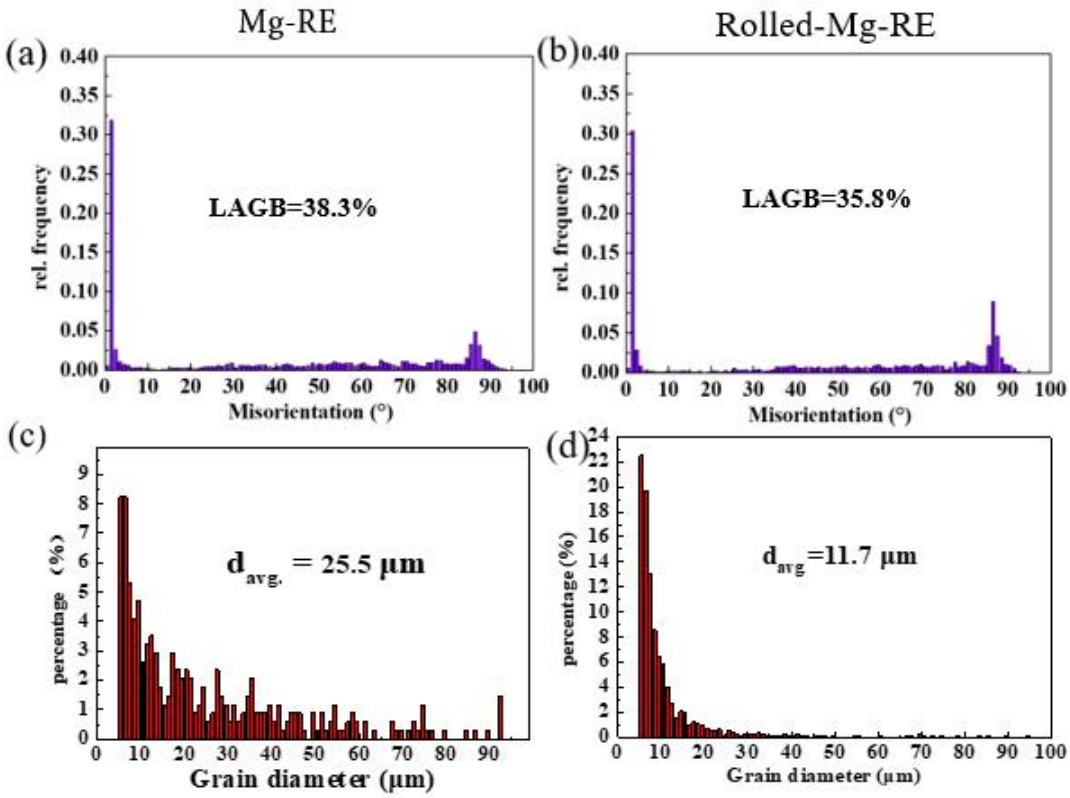

Fig. 2.11. The distributions of (a)(b) grain boundary misorientation and (c)(d) grain size.

2.5 Concluding remarks

To overcome the disadvantage of rapid degradation of biological Mg alloy, a novel Mg-based alloy with amorphous/nanocrystalline structure is designed in this chapter.

According to the three experimental principles for evaluating the amorphous forming ability, and in combination with the selection of the glass forming alloy system, we selected the rare-earth elements (Ce, La) as the components of the new Mg-based alloy material. In addition, the experimental method of producing new Mg-based alloy by VTRC process and the characterization method of microstructure are introduced in detail.

In this chapter, we studied the microstructure of four Mg-RE alloys at different casting rates. With the increase of the drawing speed, the finer the grain size of the sample, the better the corrosion resistance of the alloy. Among the four kinds of Mg-RE alloy, VTRC-30m/min Mg-RE alloy has the best corrosion resistance. Compared with VTRC-30m/min Mg-RE alloy, the local orientation error of Rolled-Mg-RE alloy is smaller with smaller grain size, and the corrosion resistance is higher.

Following the above, the experimental principles and methods involved in this study are described in detail for the convenience of understanding the experimental data and the conclusions in the following research.

Chapter 3 Animal experiment design and program of Cylindrical Mg-RE alloy

In this study, magnesium-based alloys were observed as implants in a rat femur model for more than 30 weeks. In addition, the results of bone remodeling in alloy fixation models may influence the evaluation of bone response. This part mainly introduces the types and sizes of magnesium alloys used in animal experiments, as well as the surgical procedures. The histological observation after surgery is described in detail.

3.1 Animals tests

3.1.1 Implant method

In the case of implanted alloy rods: Twenty rats were taken and divided into three groups. In this study, smooth cylindrical rods without thread and coating were used. Mg-RE rods with a diameter of 2 mm and a length of 7 mm were implanted into the femoral fixation of rats in group 1 and group 2 at a speed of 10 m/min and 30 m/min, respectively. The third group was the control group. Implants are sterilized before surgery. The size of the implant and the implantation process are shown in the figure.

In the case of implanted sheet metal: Sixteen rats were divided into four groups. In group 1 and group 2, Mg-RE and Rolled-Mg-RE tablets were implanted into the rat femur fixation model, respectively. The third group had high-purity titanium of the same size, and the fourth group had rats of the same age without implants as the control group. The sheet samples were machined into 15 mm × 5 mm with a thickness 0.5 mm. All surfaces were grounded with SiC

papers up to 1200 grid in order to ensure surface flatness and roughness. The Ti and Mg screws (4.5 mm in length, with a shaft diameter of 3.2 mm) were selected to immobilized the Ti, and the casting-rolled sheets respectively. The implant device as shown in Fig. 3.1. The implants were sterilized using ethylene oxide in an ultrasonic vibrator.

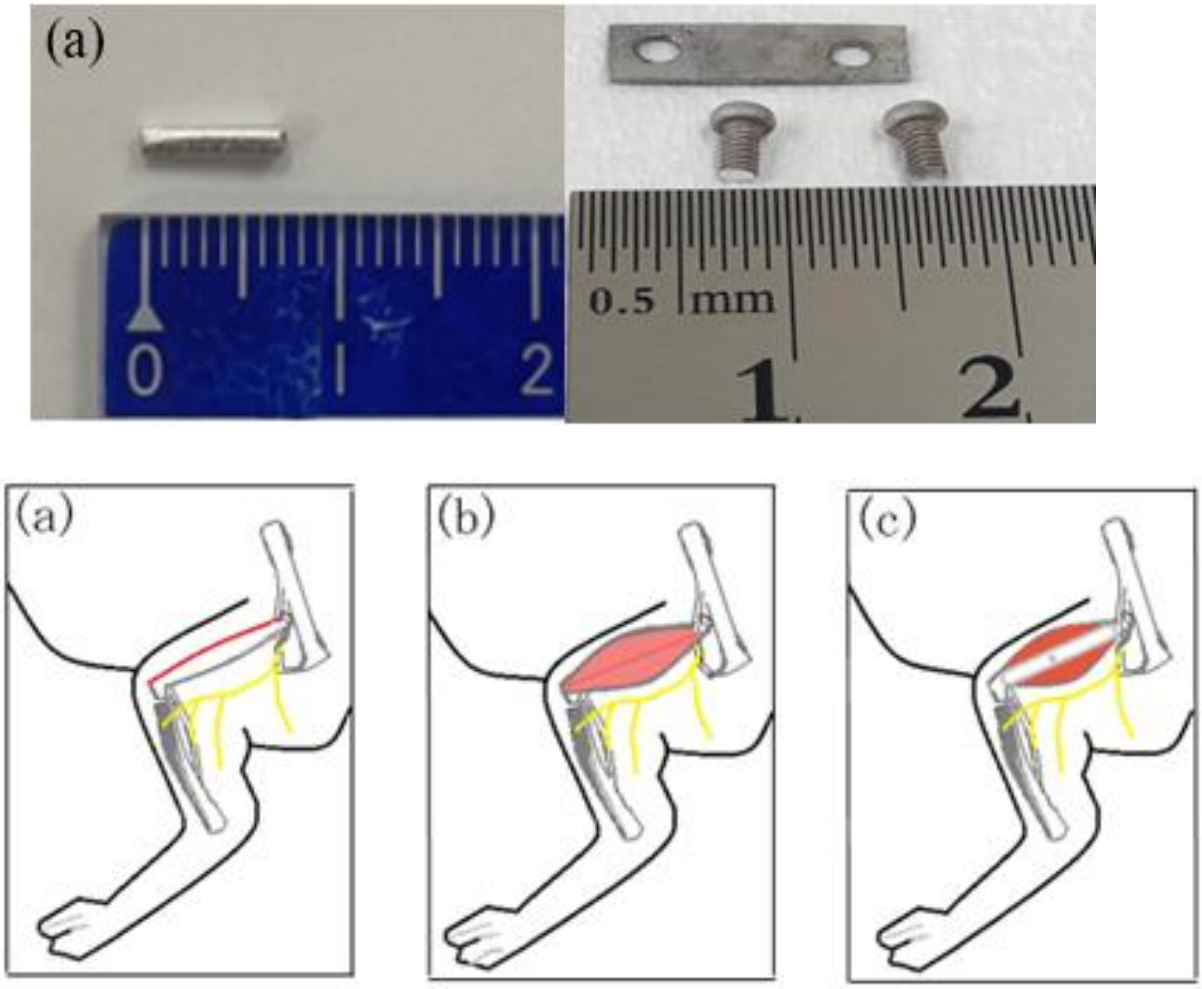

Fig. 3.1 Digital image showing implants before implantation (a); schematic diagram of cast-rolled or Ti sheets and screws fixation device with rat femoral (b).

3.1.2 Experimental animals

All animal experiments were reviewed by the Saitama Institute of Technology Animal Care and Use Committee (Grant No. 2021-2). All procedures in this study were permitted by

the Animal Institutional Review Board of Saitama Institute of Technology in accordance with the guidelines of the U.S. National Institutes of Health, and performed compliance with the Guiding Principles for the Care and Use of Animals in the Field of Physiological Sciences approved by the council of the Physiological Society of Japan. The experimental white rats (Wistar; male, 16 weeks of age, 300 ± 15 g) from Tokyo University Institute of Medicine were selected for the animal study. For micro-CT analysis and histological preparation.

3.1.3 Surgical procedure

Before surgical, all rats were anesthetized with isoflurane inhalation solution with the concentration 1% ~ 3%. The rats were placed in a lateral position and prepared for an aseptic operation on the right femur. Photographs of the surgical procedure are shown in Fig. 3.2.

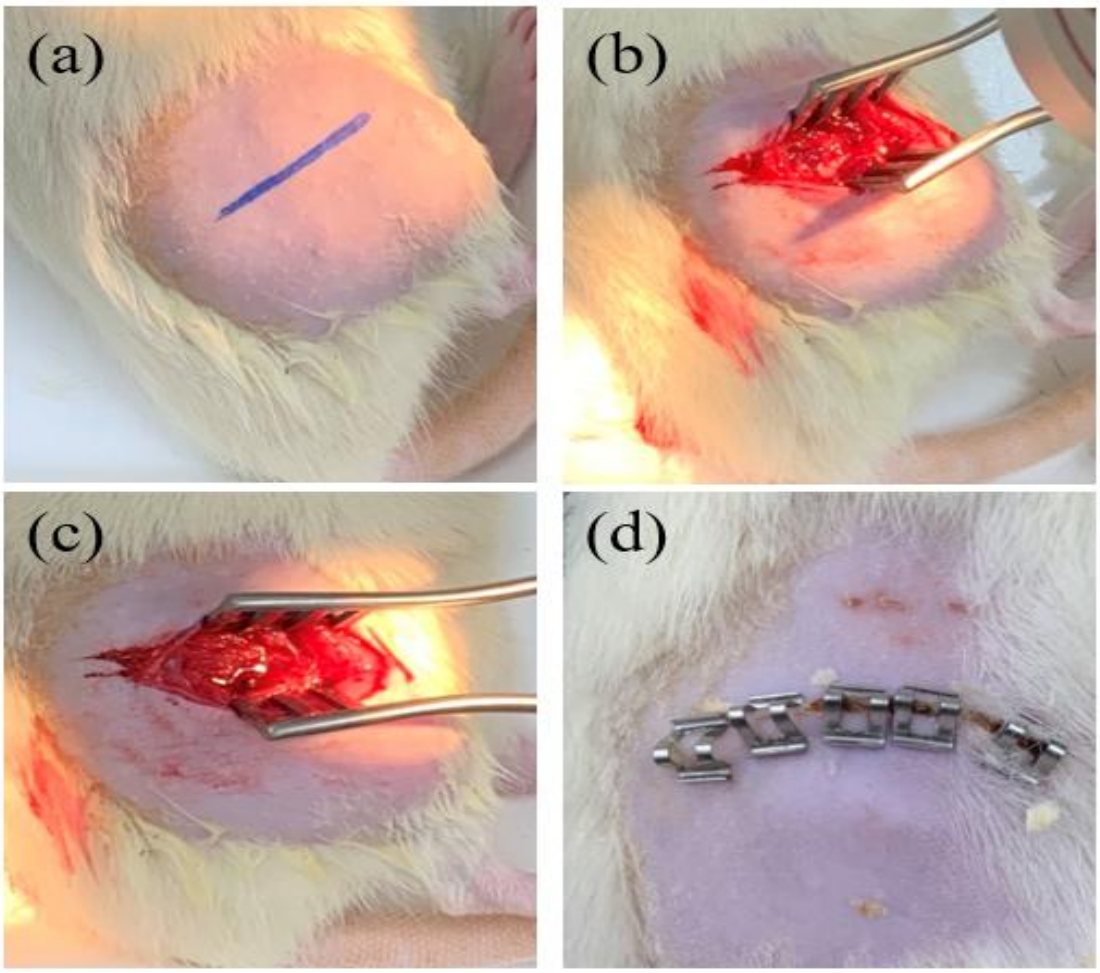

Fig. 3.2 Surgical procedure used to implant sheet implants: (a) About 20 mm incision was found on the dorsolateral side of the right hindlimb. (b) Screw holes were created in the rat femur,Drill holes and disinfection. (c) A metal rod was attached to the bone. (d) Suture the fascia to the muscle and seal the skin with a non-absorbable metal needle..

First, the right hind leg of each rat was shaved and disinfected, and a 20mm incision was made on the dorsolateral side of the right hind leg, as shown in Fig. 3.2a. The femur was then located by subcutaneous dissection. After saline cooling, a 2 mm diameter hole was drilled in the center of the femur, as shown in Fig. 3.2b. Insert the magnesium alloy rod into the hole and fix it, as shown in Fig. 3.2c. After the metal rods were implanted, the muscles and fascia were closed with absorbable monofilaments (GA03SW), and the skin was clamped with

non-absorbable metals, as shown in Fig. 3.2d. Daily clinical observation was performed after implant. Postoperative behavioral abnormalities of pain and distress, and food and water intake were observed. Intramuscular injection of buprenorphine hydrochloride (0.01 – 0.05 mg/kg three times a day for one week) and carprofen (5 mg/kg every week for four weeks) analgesics were used to suppress postoperative pain. Penicillin was used to prevent postoperative infection (0.2 mg/kg three times a day for one week).

3.2 Methods of in vivo test analysis

Micro-computed tomography (micro-CT) using a microtomographic imaging system (R.mCT2, Rigaku, Tokyo, Japan) at every two weeks evaluate device degradation and new bone formation. Image processing was performed by the 3D image processing software 3D Viewer and Volume Rendering Control. 3D volumes of the scanned devices were generated from acquired 2D lateral projections using Simple Viewer software (Fig. 3.3).

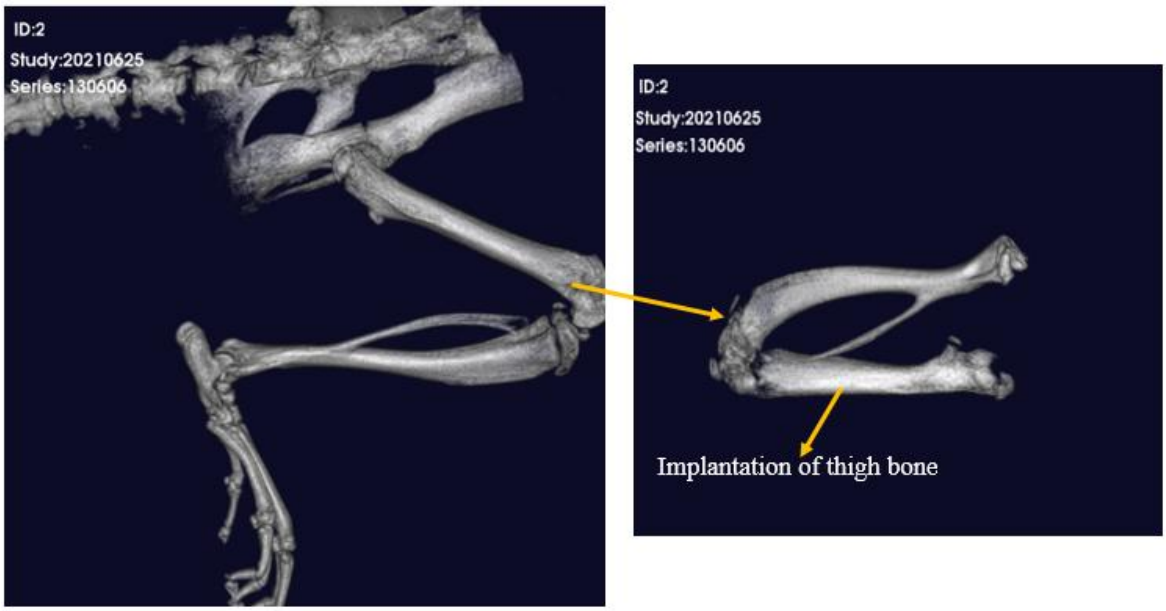

Fig. 3.3 3D images using 3D Viewer Volume Rendering software.

3.3 Histological observation method

At 8, 16 and 32 weeks, the thigh bones of the experimental rats were removed. visceral specimens were fixed in 10% formalin solution for 48 h and decalcified with (10% ethylenediamine tetra-acetic) for 28 days after operation. Next, the sample was rinsed with running water and dehydrated in a graded alcohol solution (70%, 80%, 95%, and 99% alcohol, 2 hours each). The dehydrated sample is then embedded in a paraffin block. The viscera in contact with the slice were sliced using a cut-grinding device. Finally, the specimens were stained with hematoxylin and eosin (HE), and the morphology of new bone in the experimental group were observed under the microscope.

3.5 Histological observation of visceral organs

At 8, 16 and 32 weeks, the hearts, livers and kidneys of the experimental rats were removed. The sections were made in the same way as the sections of the thigh bone, then stained with hematoxylin and eosin (HE), and finally looked at the cells of the viscera using a light microscope.

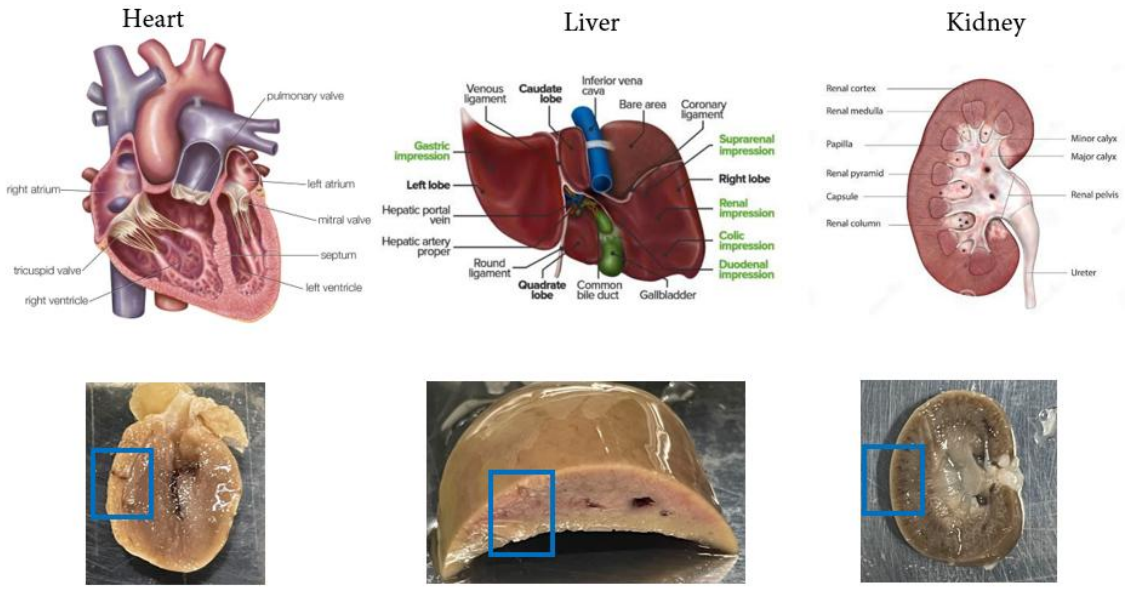

Fig. 3.4 A cross-section model of the heart, liver and kidney and a cross-section from which histological sections were made.

3.4 Concluding remarks

In the process of treating bone injury, magnesium alloy has poor corrosion resistance and is prone to excessive deterioration, which leads to the failure of the injured bone to heal. In order to overcome the rapid degradation of biomagnesium alloys, magnesium alloys must have adequate corrosion resistance, as magnesium ions must be gradually released to promote bone healing. In order to solve this problem, the effect of vertical twin-roll casting on the grain refinement of magnesium alloy and the effect of grain refinement on the corrosion resistance of the alloy were studied in the previous chapter.

In order to study whether magnesium alloy implantation can promote bone growth, animal experiments are designed and the experimental process is shown in this chapter. The alloy plate was fixed on the rat femur, and the pathological reaction of the bone tissue around the femur was observed at different time. In order to investigate whether long-term

magnesium alloy implantation would cause harm to the body, after long-term implantation, tissue samples were observed for serological diagnosis, and long-term magnesium alloy implantation was carried out in rats.

Chapter 4 in vivo degradation and bone response in a rat femur model with long-term fixation

In recent years, and magnesium alloys as metal matrix biomaterials research has attracted the attention of more and more scholars, previous studies have shown that in vivo and in vitro, magnesium alloy has good biocompatibility, biodegradation process does not produce toxic metal ions, and can be absorbed by human body [80], won't produce systemic inflammatory response, and will not affect blood cells composition [7,81-82,33]. In vitro cytological experiments also showed that it had no inhibitory effect on the growth and differentiation of mouse bone marrow cells, and could enhance the adhesion function of osteoblasts [83-84,27]. The above characteristics of magnesium and its alloy make it promising to be a new absorbable internal fixation material with sufficient mechanical strength, non-toxicity and no immunogenicity in vivo. However, in most cases, mg-based alloys with large grain sizes and many grain boundaries (GBs) are significantly limited in their wide application due to significant grain boundary corrosion [85,86]. Optimizing the microstructure of magnesium-based materials is an effective method to improve the corrosion resistance of materials. For example, casting or deformation processes can improve the corrosion resistance of mg-based alloys by refining grains and optimizing secondary phase distribution [87,88]. However, it is difficult to obtain superfine, nanocrystalline and even amorphous biodegradable magnesium alloys by traditional casting techniques.

4.1 Introduction

Compared with the traditional casting process, two-roll casting (VTRC) may be an effective method for the preparation of ultrafine, nanocrystalline or amorphous structural materials due to its fast solidification rate. In addition, VTRC process combines rolling deformation and continuous casting into one process, which has the unique advantages of high production efficiency, short production cycle and low energy consumption, and has the potential to produce sheet metal strip. Previous studies [72,89] have shown that the vertical VTRC process can produce biodegradable magnesium-based materials with nanostructures or amorphous structures. Meanwhile, previous studies [74] have shown the influence of casting process parameters on the microstructure and corrosion resistance of magnesium alloys. The research results show that among Mg-RE alloys with two speeds manufactured in vertical two-roll casting (VTRC), the Mg-RE cast-rolled parts with higher casting speed have finer grains, higher crystal-free volume fraction and higher corrosion resistance. In a 12-week in vivo experiment, Mg-RE alloy with higher casting speed was found to promote the growth of femur more. In previous studies, however, the surgery was performed with perfectly healthy bones. Therefore, further experimental studies are needed to determine whether Mg-RE has therapeutic effects on the clinical healing of fractures or bone injuries. Secondly, in clinical animal experiments, the degradation of magnesium alloy caused by long-term implantation in animals and the impact of long-term implantation on internal circulation in animals are still very limited. The proper amount of Mg element in the body can promote the normal metabolism of bone and regulate the metabolism of hormones in the body. However, excessive intake of Mg ions in the body and exclusion disorders can lead to hypermagnesia

[90-92]. Hypermagnesia can lead to the imbalance of human hormone regulation [93], liver and kidney diseases, and then neuromuscular and cardiovascular system abnormalities. Severe cases can lead to death [94]. Therefore, it is of great significance to understand the different corrosion behaviors of magnesium alloys under different casting methods and implantation methods and the effects of long-term implantation on organisms for expanding the application of magnesium based biomedical implants.

The effect of four different casting and rolling speeds on the microstructure of Mg-RE alloy was further analyzed in this study. Four magnesium alloys with different casting speeds were analyzed by electron backscattering diffraction (EBSD). In animal experiments in vivo, two representative magnesium alloys, VTRC-10m/min and VTRC-30m/min, were used to make metal rods, which were directly inserted into the femur of rats, and the Micro-CT and histological data were monitored at different times after operation. In conclusion, this study aims to provide ideas for the efficient preparation of Mg-RE alloys, and to evaluate the corrosion and bone reaction of the two kinds of Mg-RE alloys in vivo and the effects of long-term implantation on the circulation in rats, so as to judge whether they have potential application value of biomaterials.

4.2 Materials and Methods

4.2.1 Materials preparation

The experimental Mg–Re material was prepared by a copper mold casting method. Pure Mg, AZ31 ingot, Mg-10La, and Mg-20Ce (in wt.%) were used as raw materials. The melting process was conducted in an electronic resistance furnace under the protection of a CO_2 and

SF_6 mixture gas. The VTRC experiments were based on a vertical VTRC with a roll width of 100 mm, roll radius of 150 mm, and roll gap of 0 mm. When the alloy was melted completely, the melt was introduced into the roll gap between the left and right rolls via an asbestos casting nozzle. To avoid further grain growth, the cast sheet was dipped into an oil tank under the rotating rolls to quickly solidify the alloy. In this study, four casting and rolling speeds of 10 m/min, 16 m/min, 24 m/min, and 30 m/min were used.

4.2.2 Implant method

Twenty rats (Wistar; male, 20 weeks of age, 330±15g, all animal experiments were reviewed by the Animal Care and Use Committee of Saitama Institute of Science and Technology (Approval No. 2021-1), selected from the School of Medicine, University of Tokyo) and randomly divided into three groups, two of which were experimental groups. Rods with a diameter of 2mm and a length of 7mm were implanted into the thigh bones of rats, respectively. The remaining group was the control group.

4.2.3 Micro-CT and histological assessments

After 2, 8, 16, and 32 weeks of implantation, 3D models of the thigh bone and metal plates (R. M-CT. Rigaku, Tokyo, Japan) were created using micro-CT (R. M-CT) to assess new bone formation. The microstructure of the right femur was measured. Bone volume/Total volume (BV/TV) parameters were quantified using Bone-J software [6].

4.2.4 In vivo degradation tests

At 8, 16, and 32 weeks after implantation, the right thigh bone of the rats at the was

removed, and the cross section of the intersection of the implant and femur was observed using scanning electron microscopy (SEM) equipped with EDS. According to the elemental composition of the cross section, the corrosion of the two Mg–Re alloy rods in the rat and promotion of femoral growth were evaluated.

4.2.5 Histological observation

The femur specimens and visceral specimens (heart, liver and kidney) of the experimental group were fixed in 10% formalin solution for 48 h and decalcified with (10% ethylenediamine tetra-acetic) for 28 days after operation. Next, the sample was rinsed with running water and dehydrated in a graded alcohol solution (70%, 80%, 95%, and 99% alcohol, 2 hours each). The dehydrated sample is then embedded in a paraffin block. The femur and viscera in contact with the slice were sliced using a cut-grinding device. Finally, the specimens were stained with hematoxylin and eosin (H&E), and the morphology of new bone and visceral cells in the experimental group were observed under the microscope.

4.2.6 Serum diagnosis

At 4, 8, 16, and 32 weeks, 10 ml of blood was collected from the heart of each rat. The blood was centrifuged and 3 ml of the serum supernatant was sent to Yeast Industry Co., Ltd., Japan for serum diagnosis to categorize the physiological health of the rats.

4.3 Results and discussion

4.3.1 Bone response and histological examination

Fig. 4.1a shows representative 3D micro-CT reconstruction images of the rat femur 2, 8, and 16 weeks after the operation. The two Mg alloy implants remained in place, and the white part was bone and metal. A small amount of callus formation was observed at 8 weeks compared with 4 weeks after surgery. In the VTRC-10m/min group, the space around the metal rod was filled with new bone at 24 weeks; however, compared with the original bone, the growth was incomplete. In the VTRC-30m/min group, new bone formation was observed near the metal rod 8 weeks after surgery, and the space around the metal rod was completely filled with new bone at 16 weeks.

Fig. 4.1b shows a stained section of rat thigh bone 32 weeks after the operation. The bone is pink and the bone marrow is purple. The section site is the area where the metal rod was fixed (red dashed box in 4.1a). The damaged part of the thigh femur fixed with the VTRC-10m/min Mg alloy produced new bone tissue, which is still growing and has not formed a complete new bone structure. The damaged part of the thigh femur fixed with the VTRC-30m/min Mg alloy produced a large amount of bone tissue, and a relatively mature new bone structure was formed.

As shown in Fig. 4.1c, a large amount of new bone tissue was formed at the both interfaces of the Mg alloys, and the direction of bone formation was toward the implant. The increases in periosteum formation and new bone volume were similar for the two Mg alloy groups. When the mean quantitative parameters of bone morphometry were evaluated, the

Bone volume/Total volume (BV/TV) values were greater in the VTRC-30 m/min group, indicating a higher intensity of new bone formation in this rat model. Previous studies have confirmed that Mg^{2+} can promote osteocyte adhesion and bone tissue growth for new bone formation [26,28,29]. However, with the degradation of Mg-based materials, excessive ion release can inhibit the formation of new bone tissue [95], and hydrogen produced in the corrosion process can lead to tissue separation [96]. According to the EBSD analysis of several alloys, the degradation rate of the VTRC-30m/min Mg alloy is less than that of the VTRC-10m/min Mg alloy, possibly because of the high corrosion resistance of the VTRC-30m/min Mg alloy, which leads to a relatively low release rate of Mg ions. Therefore, the Mg alloy of the VTRC-30m/min group better promoted new bone formation than the VTRC-10m/min Mg alloy.

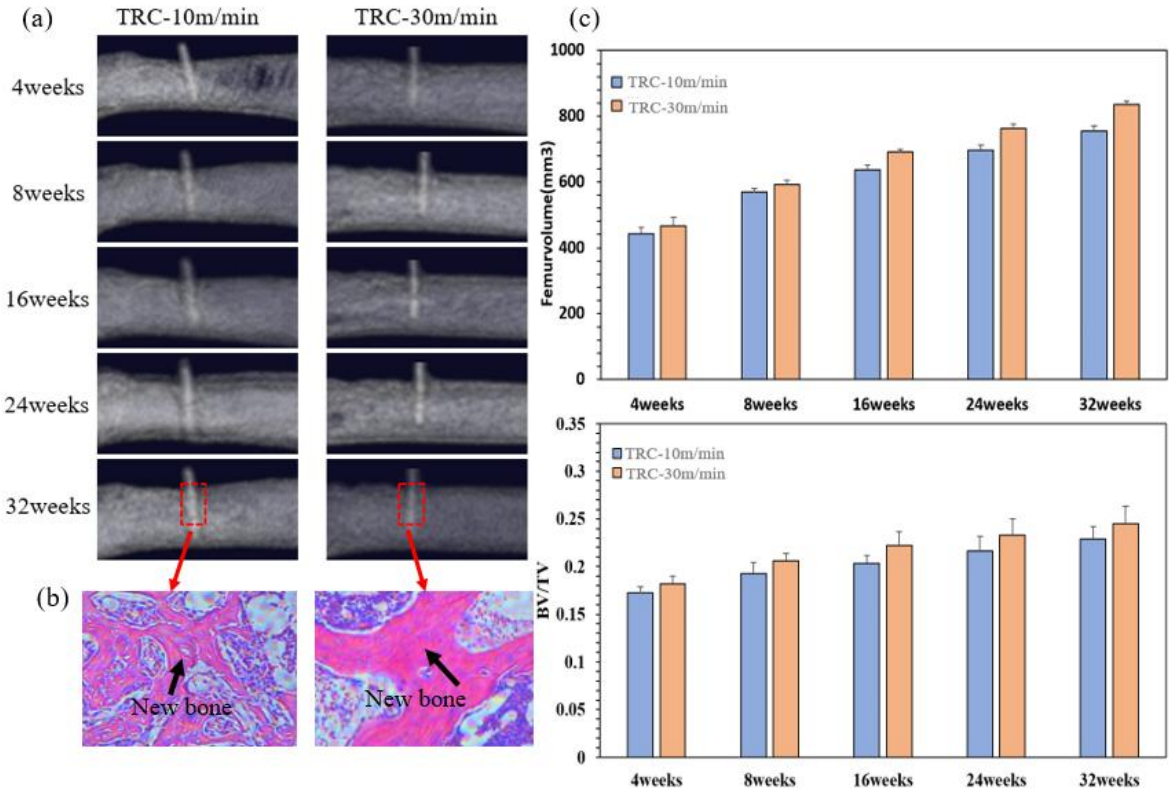

Fig. 4.1. (a) Representative 3D micro-CT reconstructions showing the bone response of the VTRC-10m/min and VTRC-30m/min Mg–Re alloy implants at 4, 8, 16, 24, and 32 weeks

after surgery. The red box is the area of interest. (b) After 32 weeks in vivo, decalcified sections were stained with hematoxylin and eosin (H&E) to visualize the morphology of the original bone and new bone around the implant. (c) Statistical analysis of the femoral parameters according to the horizontal section of interest. BV/TV: bone volume/tissue volume.

4.3.2 In vivo degradation

Fig. 4.2a shows a representative sample of the intersection of the VTRC-10m/min Mg-RE alloy rod and thigh bone 8 weeks after implantation in the rat femur, and the results of the surface EDS line scan analysis. There is a clear boundary of element distribution in the sample, which is approximately 50 μm to the left of the starting point of the line sweep. On the left side of the Mg–Re alloy of the sample, the Mg content is very high, and the content of other elements, such as Ca, P, and O, is low. The distribution of Mg elements decreases sharply as it approaches the boundary 50 μm to the left of the sample, and the distribution amplitude of Mg elements in the corrosion layer changes greatly, indicating that the Mg–Re alloy at the junction is seriously corroded and uneven. On the right side of the leg bone, the content of Mg continued to decrease slowly; however, the Ca and P content increased significantly, which is consistent with the hydroxyapatite composition of bone. In addition, the content of O is slightly greater near the junction, which may be attributed to an oxide layer at the boundary. The content of elements, such as C and Ce on both sides of the sample, is still evenly distributed, and there is no obvious boundary. Fig. 4.2b shows the results of the surface EDS linear scan analysis of the intersecting part of the VTRC-30m/min Mg–Re alloy rod and thigh bone 8 weeks after implantation in a rat femur. Elements similar to Fig. 2.5a had different trends; however, in the samples on the left side of the Mg–Re alloy, the Mg

element was close to the fast distribution of the Mg alloy in a lower leg junction. Alternatively, as shown in Fig. 2.5a, the extent of the corrosion layer of the Mg element distribution was slight, indicating the junction of the Mg–Re alloy corrosion is not serious and very even. On the side of the leg bone, the content of Mg in both samples slightly increased approximately 10 μm away from the junction, which may indicate a small amount of Mg diffused into the leg bone.

Fig. 4.2c shows the results of the surface EDS linear scan analysis of the sample at the intersection of the VTRC-10m/min Mg–Re alloy rod and thigh bone 16 weeks after implantation in a rat femur. The sample still has a clear boundary, namely the joint of the Mg–Re alloy and leg bone, approximately 60 μm to the left of the starting point of the line sweep. This indicates that there was still a small gap between the sample and rat femur. Fig. 4.2d shows the sample of the intersection part of the VTRC-30m/min Mg–Re alloy rod and thigh bone 16 weeks after implantation in a rat femur. The results of the EDS linear scan analysis showed that there was no obvious boundary in the sample, indicating that there was no gap between the Mg–Re alloy rod and femur and it was filled with new bone. Moreover, the Mg distribution at the joint of the Mg–Re alloy rod and femur was relatively uniform, indicating that the Mg element in the Mg–Re alloy was partially and uniformly diffused into the femur.

Fig. 4.2e shows the results of the surface EDS linear scan analysis of the sample at the intersection of the VTRC-10m/min Mg–Re alloy rod and thigh bone 32 weeks after implantation in a rat femur. The sample still has a boundary with the joint of the Mg–Re alloy and leg bone approximately 25 μm to the left of the starting point of the line sweep. This

indicates that there was still a small gap between the sample and rat femur. Fig. 4.2f shows the sample of the intersection of the VTRC-30m/min Mg–Re alloy rod and thigh bone 32 weeks after implantation. The results of the EDS scan analysis show that there was no obvious boundary in the sample, and Mg elements were relatively evenly distributed at the junction of the Mg–Re alloy rod and femur. The Mg element in the Mg–Re alloy partially and uniformly diffused into the femur, and the content of Mg element in the junction of the Mg–Re alloy and femur was significantly greater than that in the VTRC-30m/min Mg–Re alloy 16 weeks after implantation.

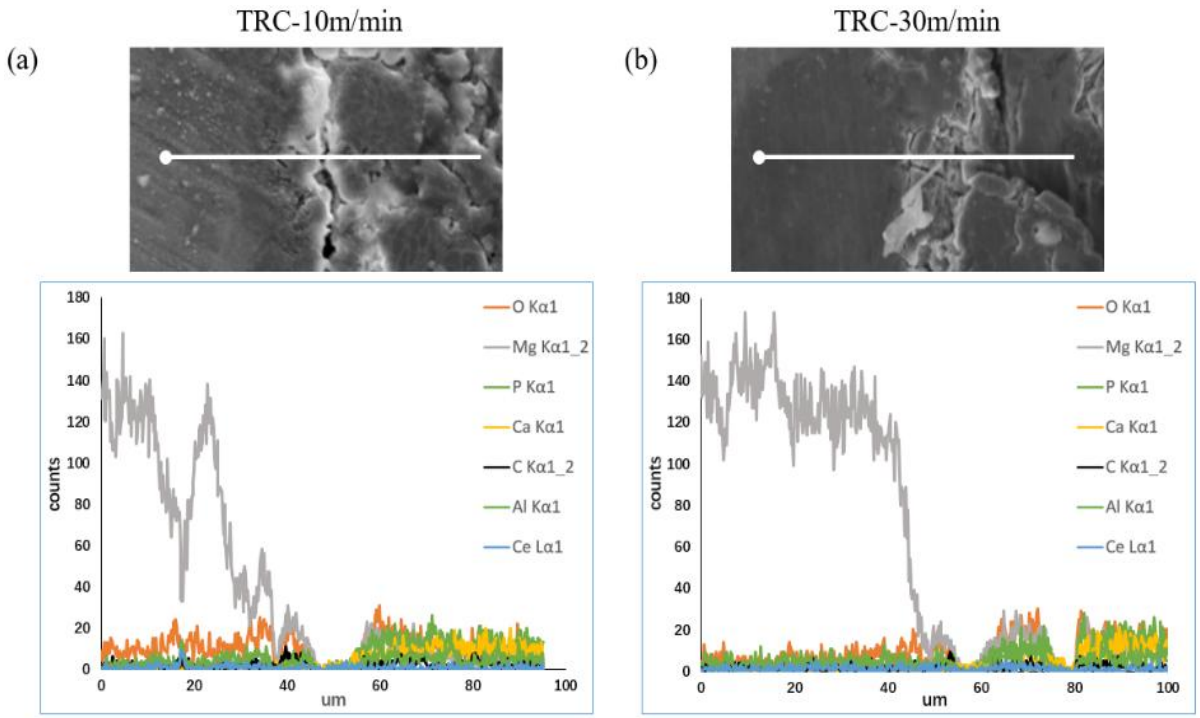

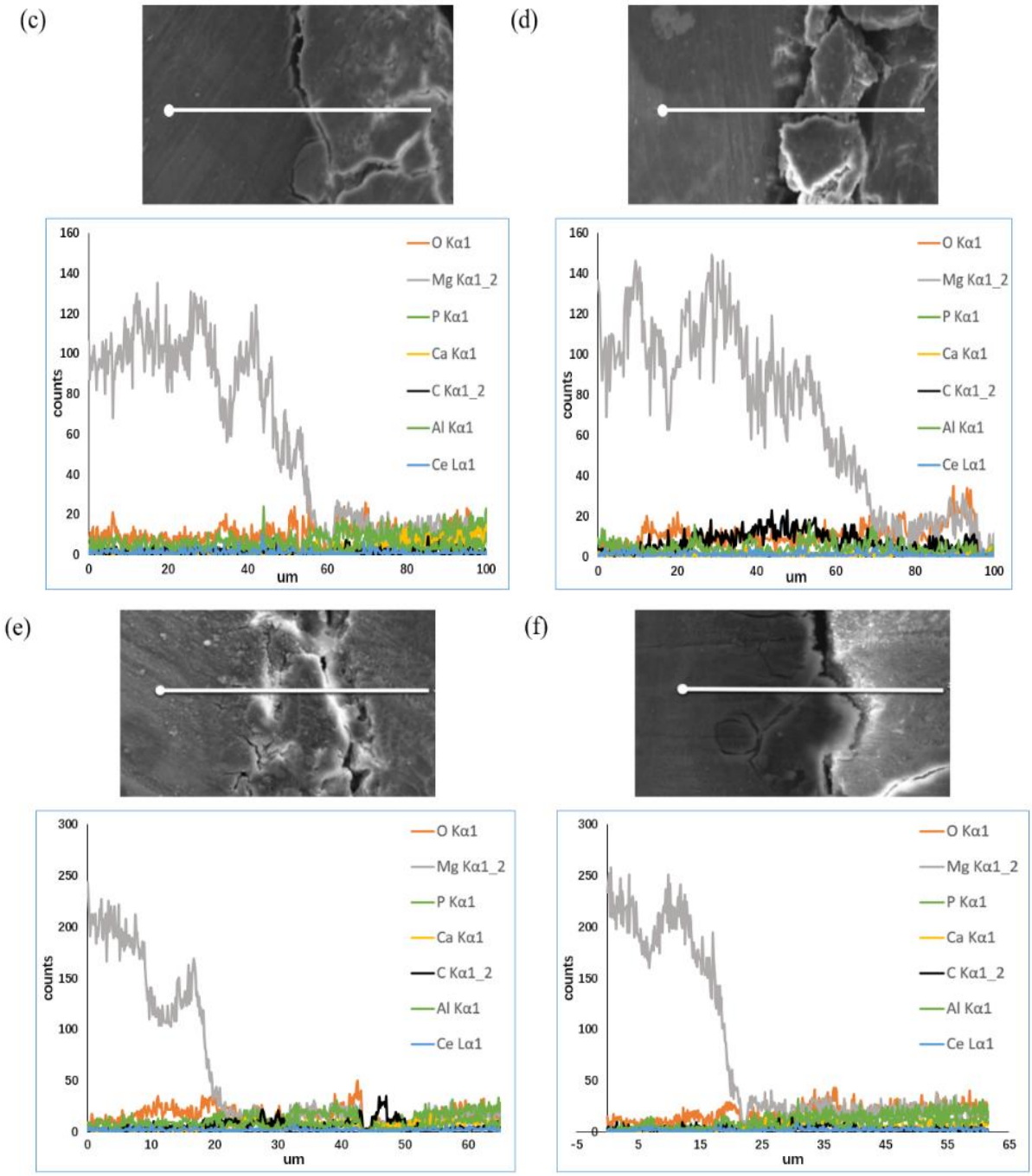

Fig. 4.2. EDS line scanning observations of the (a) (c) (e) VTRC-10m/min and (b) (d) (f) VTRC-30m/min magnesium alloys and intersecting bone sections at 8, 16, and 32 weeks of implantation.

4.3.4 Histological examination after implantation

To evaluate the biocompatibility of the two Mg alloys in vivo, we evaluated the histocompatibility of representative samples of the liver, myocardium, and kidney. As shown

in Fig. 4.3, compared with the Control group, there was no significant difference in the size and morphology of cells and nuclei of the VTRC-10m/min group and VTRC-30m/min group. No necrotic tissue was observed. No morphological changes, edema, or degeneration were observed in the endomyometrium and nucleus of myocardium. Clear and intact proximal convoluted tubules were observed in the kidney specimens, indicating no inflammation or tissue damage in either group. Hepatocytes in the VTRC-10m/min group were obviously injured, and with an increase in time in vivo, the larger the area of the vacuoles, the greater damage, while hepatocytes in the VTRC-30m/min group had a normal structure and no signs of damage. According to the implant corrosion analysis, the implants in the VTRC-10m/min group corroded too fast and released too much Mg, which caused hepatocyte injury.

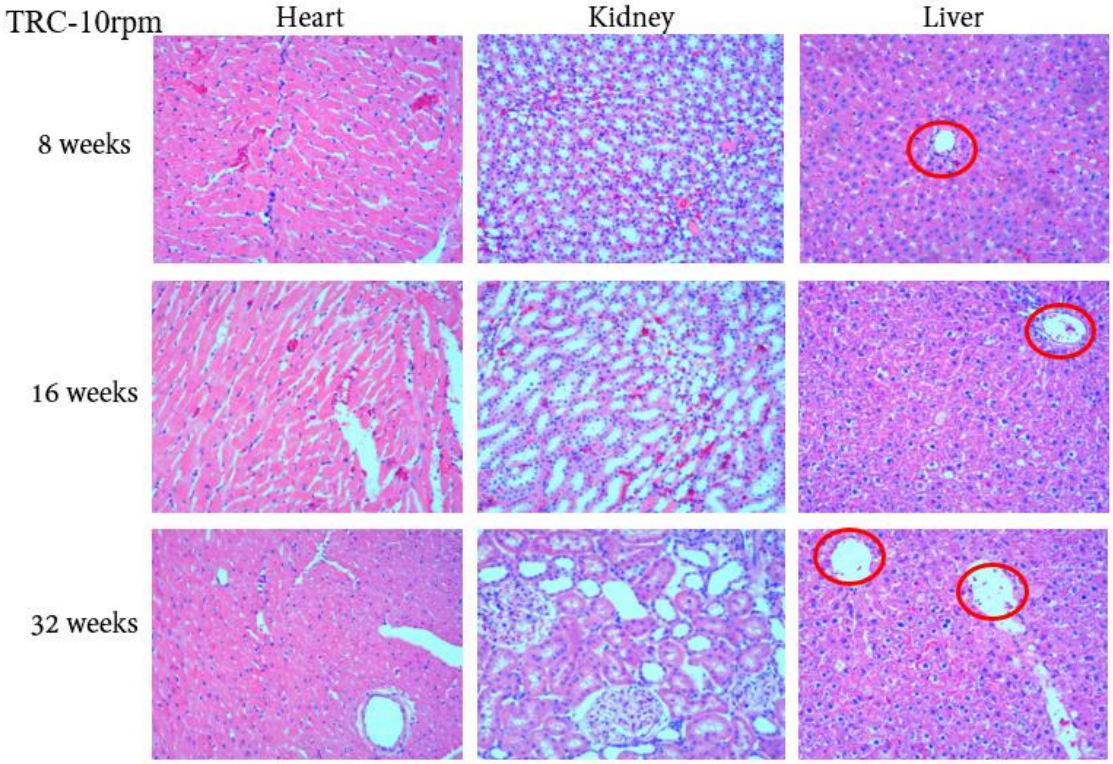

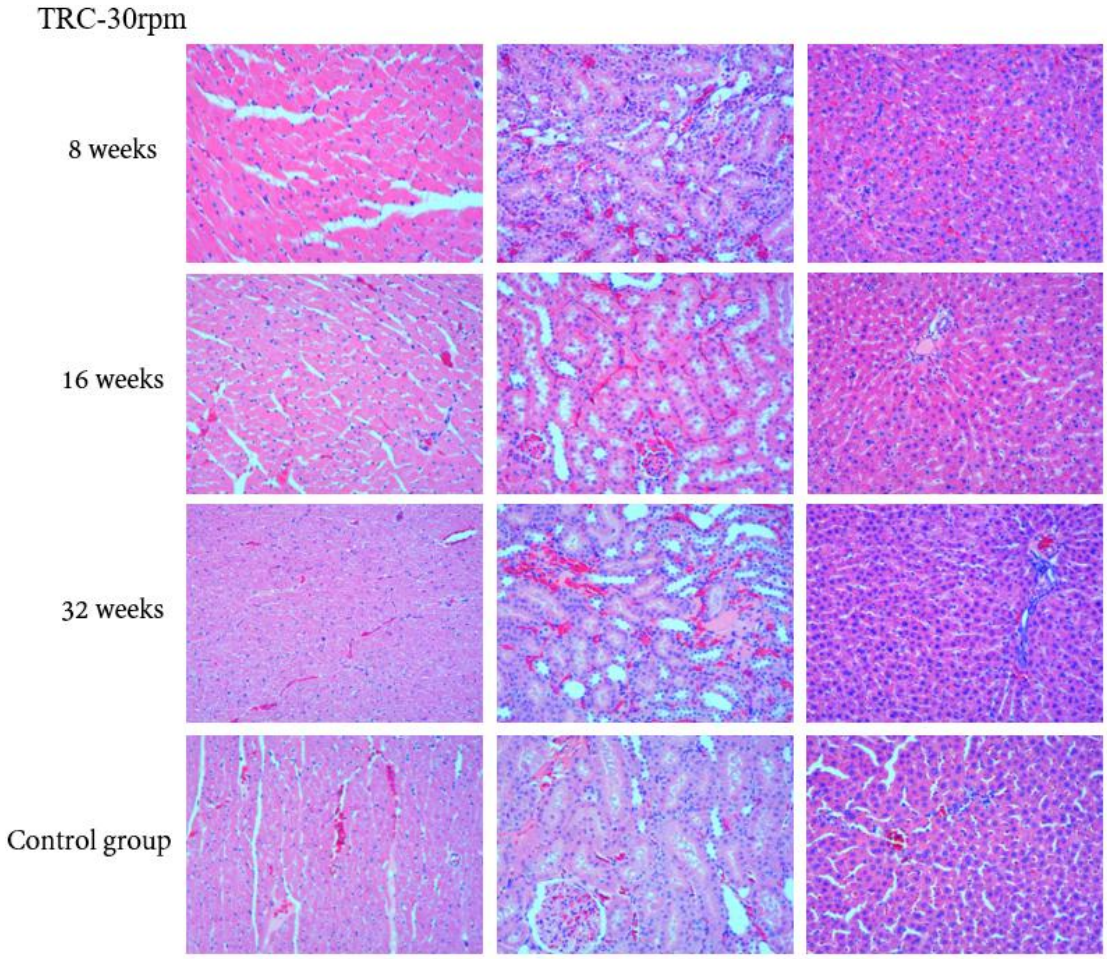

Fig. 4.3. Representative HE staining of liver, myocardium, and kidney tissue 8, 16, and 32 weeks after implantation.

4.3.5 Serum test results

As shown in Fig.4.4, during the implantation process, the values of aspartate aminotransferase (AST) and alanine aminotransferase (ALT) in the Control group and VTRC-30m/min group were similar. AST and ALT are indicators of early myocardial infarction, hepatocyte necrosis, degeneration, liver cirrhosis, liver cancer, and other diseases, indicating that the liver function of rats in the VTRC-30m/min group did not change significantly because of the alloy, while the amount of AST and ALT in the VTRC-10m/min group was greater than that in the Control group over the entire in vivo period. The reason for

this change may be that the Mg alloy in the VTRC-10m/min group decomposed too fast 8 and 16 weeks after implantation in the rat thigh bone, leading to an excessive Mg ion concentration in the body, thus causing damage to the liver function that is consistent with the results of the visceral sections of rats in the experimental group.

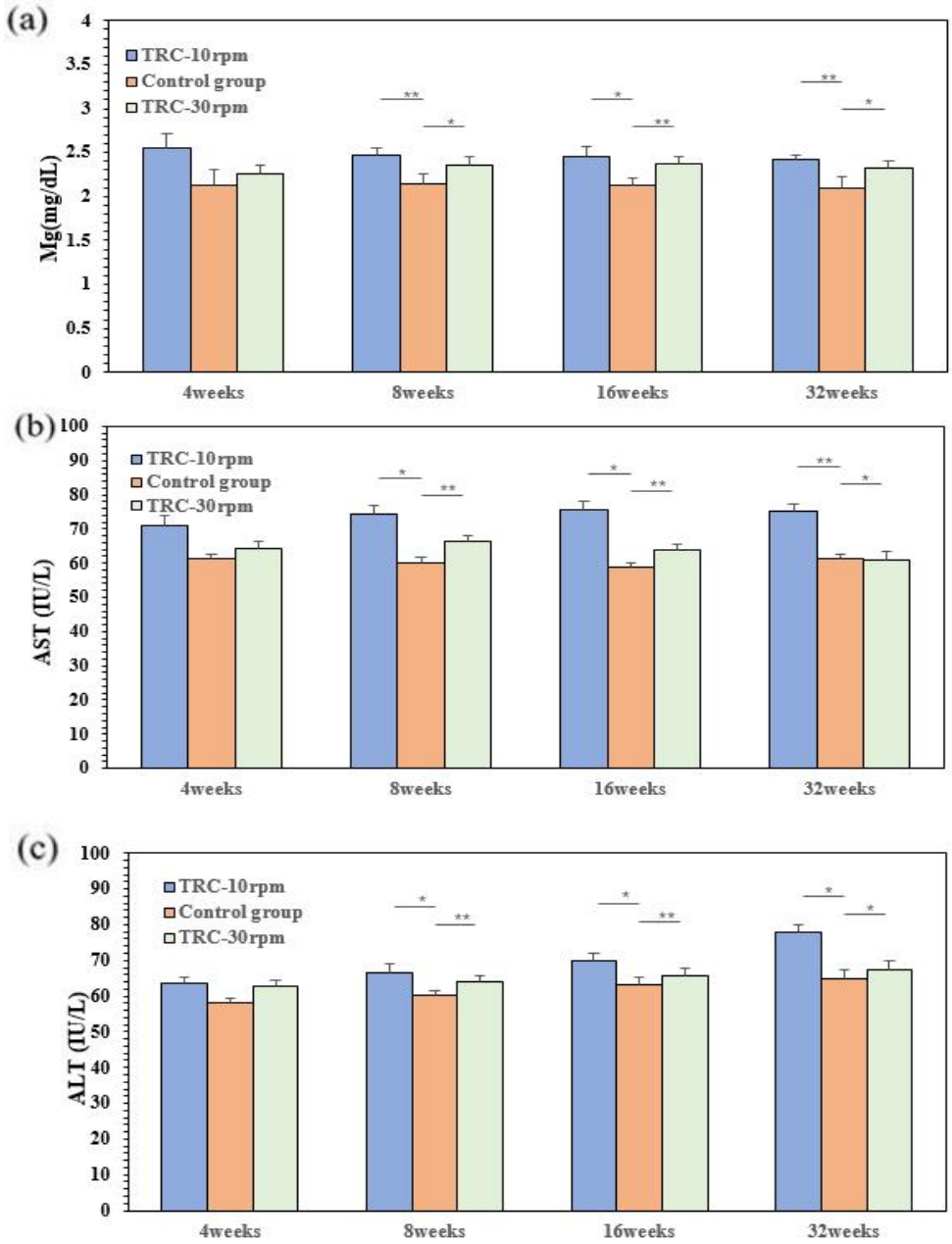

Fig. 4.4. Mg^{2+} concentration and main liver function indexes of experimental animals at 4, 8, 16 and 32 weeks after operation.

4.4 Concluding remarks

In this study, four Mg alloys were obtained using vertical two-roll casting (VTRC) at 10 m/min, 16 m/min, 24 m/min, and 30 m/min, and their microstructure, corrosion behavior and bone reaction in vivo were studied. The corrosion resistance of the alloy increases with an increase in casting speed and finer grain size of the cast-rolled parts. The Mg–Re alloys with VTRC-10 m/min and VTRC-30m/min were selected for animal experiments. The two Mg alloys were made into metal rods and inserted into the rat femur to simulate the effect of Mg–Re on femoral healing under an injury condition. The rods were implanted for a long time to judge the effects of the Mg–Re alloy on the body. The VTRC-30m/min implants obtained highly mature new bone tissue in the case of bone injury. In vivo experiments showed that the corrosion resistance of the VTRC-30m/min implant was better than that of the VTRC-10m/min implant. After 32 weeks of implantation, there were no pathological changes in the liver, heart, or kidney of rats in the VTRC-30m/min group, and the cell structure was normal.

Chapter 5 In vivo degradation and bone reaction of long-term fixation with twin-roll casting Mg alloy in a rat femur model

Bone transplantation is one of the most frequently performed tissue transplantation procedures worldwide, second only to clinical blood transfusions. Metal materials play a very important role in treating orthopedic injuries or replacing bone tissue in modern medicine [97]. Magnesium alloys have higher mechanical strength and fracture toughness, and are more suitable for load-bearing applications. Compared with stainless steel, titanium, and cobalt-chromium alloy, Mg metal has better biocompatibility, does not produce toxic metal ions in the degradation process, can be absorbed by the human body, and does not require a second operation to remove, greatly reducing medical costs and patient pain. In addition, Mg is an essential element to maintaining daily activity, accounting for approximately 0.05% of the total body weight, more than half of which exists in the skeleton. Various in vitro and in vivo experiments have proven that Mg has good biocompatibility and biosafety [23,25,98]. However, pure Mg corrodes too quickly under normal physiological conditions, losing mechanical integrity before bone tissue can properly heal, and producing hydrogen faster than the host tissue can process [46,99]. Therefore, although magnesium as an orthopedic implant has had some success, there is still room for development.

In the past ten years, Mg alloys containing rare earth elements have attracted attention. The addition of rare earth elements such as Y, La, Ce, Nd, Sm and Gd improves the plasticity and strength of the Mg alloy, and reduces the anisotropy and tension/compression asymmetry of the magnesium alloy compared with AZ31 and other common Mg alloys [100-103]. In addition to improving the ductility and strength, Mg alloys containing rare earth elements also

have high creep resistance and corrosion resistance [104-106]. In addition to the alloy composition, the corrosion resistance of Mg is also affected by its internal microstructure characteristics such as the grain boundary (GB) [107-109], precipitated phase [110-112], grain orientation [113-116], and dislocation [117]. Most biodegradable Mg alloys are deformed alloys, and their mechanical properties are superior to casting alloys because of the fine grain strengthening effect produced by plastic deformation [118,119].

5.1 Introduction

Previous studies prepared magnesium rare earth (Mg-RE) alloy sheets using a vertical two-roll continuous casting machine (VTRC). Microscopic characterization experiments show that the resulting crystal structure is amorphous. Moreover, Mg-RE has better corrosion resistance than intermediate alloys [120]. However, the effect of casting parameters on the microstructure and corrosion resistance of Mg alloys is still limited, especially in clinical animal experiments. Understanding the corrosion behavior of magnesium alloys in different casting methods is of great significance for expanding the application of Mg-based biomedical implants.

On the basis of previous studies, a Mg-RE alloy was prepared by the VTRC process, and an Rolled-Mg-RE alloy was prepared by rolling the Mg-RE alloy. The microstructures, in vivo degradation behaviors, and bone reactions of Mg-RE (Ce, La), Rolled-Mg-RE, and titanium implants were observed in a rat femoral model for up to 48 weeks. The long-term effects of the new Mg-RE alloy on biological systems and local vital organs were further analyzed.

5.2 Methods

5.2.1 Implant method

Sixteen rats (Wistar; male, 30 weeks of age, 370±15g, all animal experiments were reviewed by the Animal Care and Use Committee of Saitama Institute of Science and Technology (Approval No. 2020-1), selected from the University of Tokyo Medical School) and randomly divided into 4 groups. The rectangular Mg-RE and Rolled-Mg-RE tablets with the thickness of 4 mm × 13 mm and 0.5 mm were implanted into the femoral fixation model of rats in groups 1 and 2, respectively. The third group was high purity titanium of the same size, the fourth group was the same age rats without implants as control. All Mg alloy implants were fixed with AZ31 screws and titanium implants were fixed with titanium screws. The implants were disinfected with ethylene oxide before surgery. The implantation process is shown in Fig. 5.1. Daily clinical observations were performed after surgery.

The femur and viscera of rats with high purity titanium and the Mg alloys were implanted 48 weeks after operation. Micro-CT, histological, and physiological analysis were performed. The alloy sheets were explanted and the microstructure was analyzed.

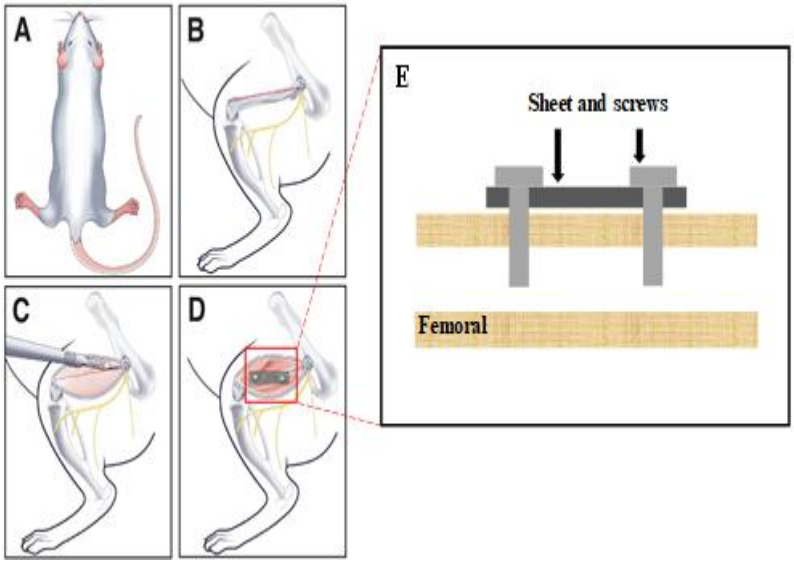

Fig. 5.1. The implant surgery was performed in Wistar rats: (a) anesthetized rats; (b) mark the corresponding implant location; (c) drill holes in the femur of rats; and (d) fixation of alloy plates with bone screws.

5.2.2 Micro-CT analysis

Micro-CT was used to evaluate implants degradation and the formation of new bone. Image processing was performed by means of 3D Viewer and Volume Rendering Control. 3D volumes of the scanned devices were generated from acquired 2D lateral projections using a Simple Viewer software. after implantation for 2, 8, 16, 32, and 48 weeks, 2D cross-sections and 3D models of the thigh bone and metal plates were taken using micro-CT (R. m-Ct. Rigaku, Tokyo, Japan) to evaluate the formation of new bone.

5.2.3 In vivo degradation tests

48 weeks after implantation, the rats were dissected and the implanted metal was removed from the thigh bone. Field emission scanning electron microscopy (FE-SEM, JMS-6301, Japan) was used to observe the cross section morphology of the Mg-RE plate. The cross section of the implant was observed by scanning electron microscopy to analyze the structure of the degradation layer and the degradation characteristics of the two Mg-RE plates.

5.2.4 Histological observation

The femur specimens and visceral specimens (heart, liver and kidney) of the experimental group were fixed in 10% formalin solution for 48 h and decalcified with (10% ethylenediamine tetra-acetic) for 28 days after operation. Next, the sample was rinsed with running water and dehydrated in a graded alcohol solution (70%, 80%, 95%, and 99% alcohol, 2 hours each). The dehydrated sample is then embedded in a paraffin block. The femur and

viscera in contact with the slice were sliced using a cut-grinding device. Finally, the specimens were stained with hematoxylin and eosin (H&E), and the morphology of new bone and visceral cells in the experimental group were observed under the microscope. Liver sections were stained by PAS staining, also known as periodate schiff staining and glycogen staining, to reveal glycogen and other polysaccharides.

5.2.5 Serum diagnosis

After surgery, 10 ml of blood from the heart of rats in each group was taken. The blood was centrifuged and 3 ml of the serum supernatant was sent to Yeast Industry Co., Ltd., Japan for serum diagnosis to categorize the physiological health of the rats.

5.3 Results and discussion

5.3.1 Bone response and histological examination

Fig. 5.2a shows micro-CT images and 2D cross-sectional images of the thigh bone of rats implanted with the Mg alloys and titanium. During the corrosion process of the Mg-RE plate during implantation, a small amount of new bone formed between the bone and Mg alloy lamina 4 weeks after surgery, and further growth was observed at 12 weeks. After 24 weeks, the boundary between the plate and bone became blurred because of new bone tissue. After 48 weeks, the Mg alloy plate and bone end gap were nearly completely covered by new bone. In the corrosion process of the Rolled-Mg-RE plate, a small amount of new bone also appeared 4 weeks after surgery and continued to grow. At 48 weeks, the Mg alloy plate and bone end gap were nearly completely covered by new bone. During the corrosion of the titanium plate implants, numerous biological tissues appeared on the Ti screws and Ti plates at 8 weeks and 24 weeks postoperative. No significant new bone tissue was formed

continuously between the lamina and bone. After 32 weeks and 48 weeks of surgery, the biological tissue on the titanium screw and plate disappeared and no signs of new bone growth were observed. Four weeks after surgery, the boundary between the Ti plate and thigh bone was more obvious than that between the two Mg alloy plates. On the basis of the increase in corrosion time, the bone growth of the two Mg alloy plates was better than that of the Ti plate.

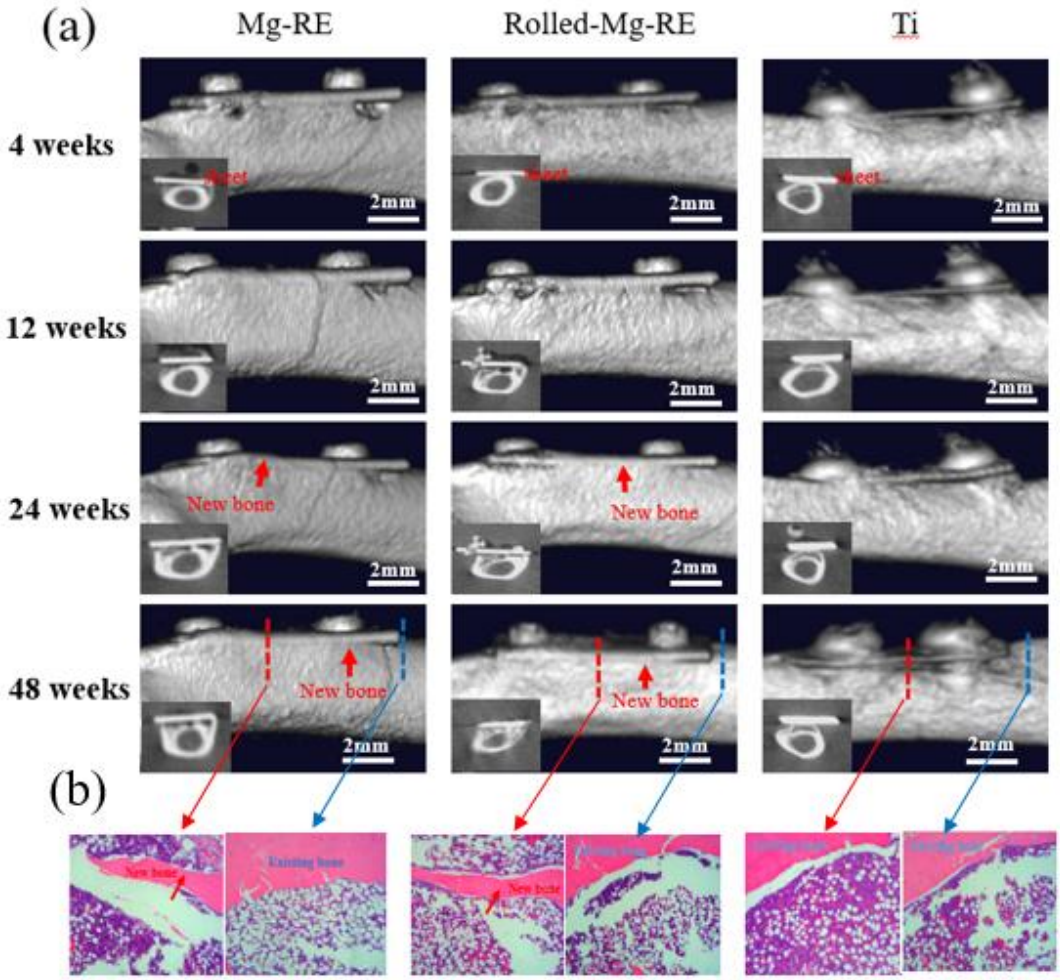

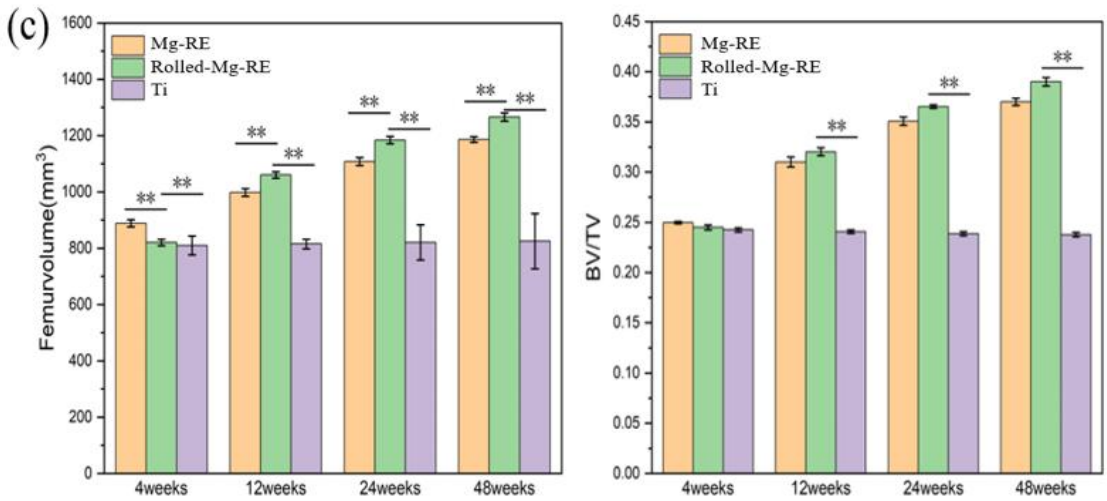

Fig. 5.2. (a) Representative 3D micro-CT reconstructions showing bone response at 4, 12, 24, and 48 weeks postoperative with thin Ti, Mg-RE, and Rolled-Mg-RE implants. Red box is the area of interest. (b) Implants after 48 weeks with hematoxylin and eosin (H&E) staining of decalcified sections showing the morphology of existing and new bone around the implant. The blue box represents the part of bone not in contact with the implant and the stained section of this part. (c) Femur parameters were statistically analyzed according to the horizontal section area of interest. BV/TV: bone volume/tissue volume (*P < 0.05, **P < 0.01).

Fig. 5.2b shows the stained section of rat thigh bone after 48 weeks, with bone pink and bone marrow purple. Starting from the central part of the fixed metal (red dotted box in 5a), some of the bones in the fixed Mg alloy changed shape significantly, forming a mature new bone structure, while the bones and marrow did not change at all in the thigh bone of the unfixed Mg alloy plate (blue dotted box in 5a). No significant changes in bone or marrow were observed in the fixed titanium plates.

Fig. 5.2c shows that a large mature new bone structure was formed at the interface of the two Mg alloys, and the direction of bone formation was toward the implant. The periosteum formation and femur volume increase of new bone were similar between the two Mg alloy groups. At 4 weeks, the increased volume of femur implanted with the Mg-RE plate was greater than that with the Rolled-Mg-RE plate, and at 12 weeks, the increased volume of the femur with the Rolled-Mg-RE plate was greater than that with the Mg-RE plate. Previous

studies confirmed the beneficial effect of Mg^{2+} on new bone formation, promoting bone cell adhesion and bone tissue growth [121-124]. According to the SEM analysis of EBSD in this study, the degradation rate of Rolled-Mg-RE is less than that of the Mg-RE plate because of the higher corrosion resistance of the Rolled-Mg-RE plate. With the plate degradation, Mg^{2+} stimulates local tissue, forming new bone. Therefore, the femoral volume around the implanted Mg-RE plate was greater than that of the Rolled-Mg-RE plate and titanium. However, with Mg base material degradation, excessive ion release can inhibit the formation of new bone tissue [125] from implantation through 12 weeks. The increase in femur volume after implantation of the Rolled-Mg-RE plate was greater than that with the Mg-RE plate and titanium plate. In this study, the surgery was performed when the bones were completely healthy. Therefore, whether Mg-RE has a therapeutic effect on the clinical healing of a fracture or bone injury needs further study. No significant changes were observed near the femur after implantation of the nonabsorbable titanium, which rules out external factors that may cause bone remodeling by altering the mechanical load of the implant.

According to these research results, there is a relationship between different casting methods and the properties of the Mg-RE alloys, including biological conditions. The rolled Mg-RE alloy can produce larger grain size and lower orientation deviation, which improve the corrosion resistance of an Mg alloy. In vivo results confirmed that the Rolled-Mg-RE alloy had better bone formation ability and corrosion resistance over long term implant.

5.3.2 In vivo degradation

Fig .5.3 shows the representative cross section of the alloy sample and the corresponding SEM image. Characteristic corrosion layers of the two Mg alloys were observed as double layers. Degradation layers of different thickness were observed in the Mg alloys. The inner thickness of the Mg-RE alloy was approximately 30 μm and the outer thickness was

approximately 45 μm. In addition, there were microcracks in both the inner and outer layers. Microcracks may be caused by accelerated dissolution of the degradation products. After rolling, the inner thickness of the Rolled-Mg-RE alloy was approximately 10 μm, and the outer thickness was 40 μm. The double layer structure was dense and uniform, and no obvious microcracks were observed.

Mg and its alloys dissolves in body fluids based on following equations:

$Mg \rightarrow Mg^{2+} + 2e$; anodic reaction.

$2H_2O + 2e \rightarrow H_2 + 2OH^-$; cathodic reaction.

$Mg + 2H_2O \rightarrow Mg(OH)_2 + H_2$; Overall reaction.

$Mg(OH)_2$ changes $MgCl_2$ under the action of the cathodic ion (Cl^-), which can increase the PH of the solution and result in further dissolution of Mg [126,127]. Furthermore, Ca^{2+} and PO_4^{3-} in body fluids reacts with OH^- to form $Ca_{10}(PO_4)(OH)_2$ [128,129]. Previous research [130-132] report studied Mg and C, O, P, Ca and other elements in the corrosion layer. It is proved that these degradation products can promote newly formed bone and show good biocompatibility. Therefore, it could be concluded that the degradation product of the Mg-RE alloy is acceptable and good. However, the dissolution mechanism of the degradation layer remains to be further studied. Mg and other elements such as C, O, P and Ca in corrosion layer were studied.

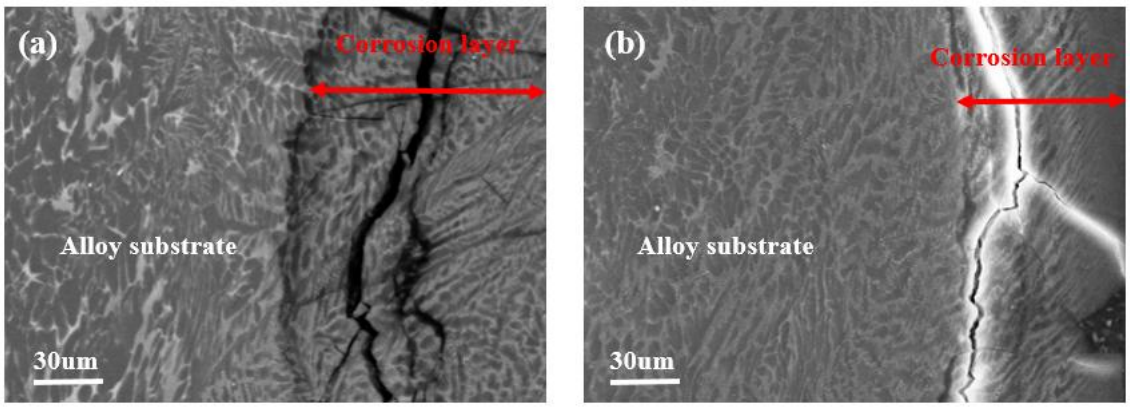

Fig. 5.3. SEM images of alloy plates implanted in rat thigh bone after 48 weeks: profiles of the degradation layer of (a) the Mg-RE alloy and (b) Rolled-Mg-RE alloy.

5.3.3 Histological examination after implantation

Fig. 5.4 shows the histological appearance of the liver and heart after 48 weeks in vivo. The size and morphology of cells and nuclei in the experimental groups and control group have no significant difference. The rats implanted with Mg alloy for a long time had no liver injury and normal liver cell structure, similar to the rats without a Mg alloy. Compared with the control group, the experimental group showed no morphological changes and no edema of the myocardium and nucleus after HE staining. No inflammation or tissue damage was observed in the three experimental groups.

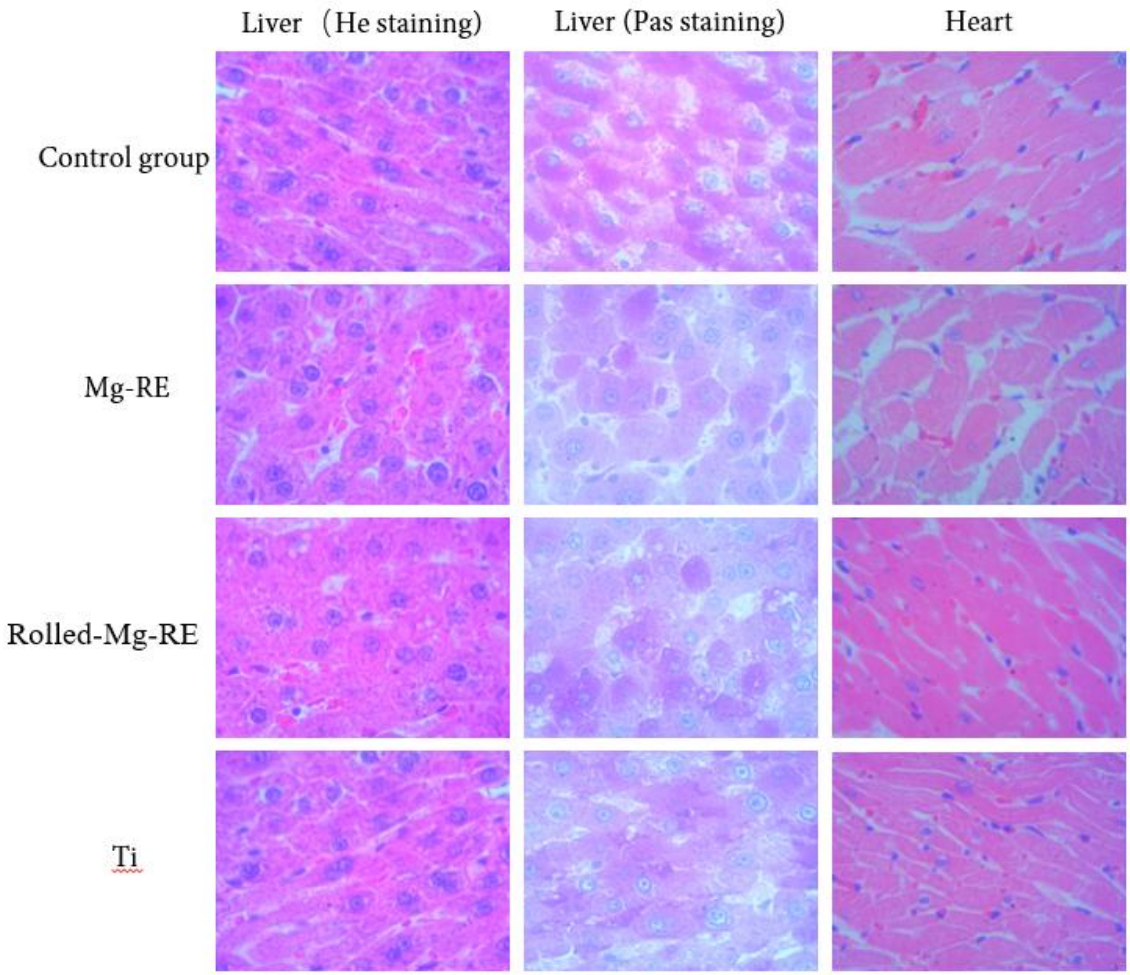

Fig. 5.4. Representative HE staining and PAS staining of the liver and representative HE staining of the myocardium 48 weeks after transplantation.

4.3.5 Serum test results

There were no significant differences in total protein, albumin, total cholesterol, triglyceride, and glucose between the control group and titanium alloy group. The concentrations of sodium, potassium, chloride, calcium, and magnesium in the serum of the four groups were measured. The concentration of Mg ions in the Mg alloy group were slightly greater than those in the other groups. Elevated creatinine levels indicate decreased kidney function. Slightly higher concentrations of creatinine were observed in rats with rolled Mg alloys, which may be associated with higher concentrations of Mg ions. The AST(glutamic oxalacetic transferase) and ALT(glutamic-pyruvic transaminase) values of the control group, titanium alloy group, and two Mg alloy groups were similar, AST and ALT are indicators of early myocardial infarction, hepatocyte necrosis, degeneration, cirrhosis, liver cancer and other diseases , the liver function of rats in these groups did not change significantly because of the alloy implantation.

Table. 5.1. Serum test results of rats 48 weeks after implantation of the Mg alloys, titanium, and control

	TP (g/dL)	ALB (g/dL)	CRE (mg/dL)	Na (mEq/L)	K (mEq/L)	Cl (mEq/L)	Ca (mg/dL)	Mg (mg/dL)	AST (IU/L)
Control group	6.2	4.2	0.32	138	5.1	98	9.8	2.1	59
Ti	6.5	4.4	0.33	145	4.6	104	9.7	2.1	72
Rolled-Mg-RE	6.3	4.3	0.37	138	5.4	97	10.1	2.5	57
Mg-RE	6.2	4.3	0.35	140	4.6	100	10	2.2	54
	ALT (IU/L)	LDH (IU/L)	AMY (IU/L)	r-GT (IU/L)	T-CHO (mg/dL)	TG (mg/dL)	HDL-C (mg/dL)	T-BIL (mg/dL)	GLU (mg/dL)
Control group	36	288	1389	3＞	100	361	28	0.07	373
Ti	31	290	1492	3＞	92	338	29	0.06	303
Rolled-Mg-RE	36	277	1436	3＞	112	292	34	0.06	317
Mg-RE	34	251	1499	3＞	121	342	30	0.08	336

5.4 Concluding remarks

In this study, a new magnesium rare earth alloy (Mg-RE, where Re is Ce or La) was prepared by vertical two-roll casting and Rolled-Mg-RE was prepared by further rolling. The microstructure characteristics, degradation behavior, and bone reaction of the two alloys were studied. The microstructure shows that the local orientation error of Rolled-Mg-RE is less than that of Mg-RE. The local orientation error within the grain leads to a higher corrosion rate; as a result, Rolled-Mg-RE has better corrosion resistance. Ti, Mg-RE, and Rolled-Mg-RE alloy plates were implanted in a rat femur model, and their degradation behavior was observed 48 weeks later. In vivo experiments showed no significant changes around the femur in the Ti group, excluding external factors that may cause bone remodeling and lead to new bone formation. Rolled-Mg-RE induces more new bone formation than Mg-RE, which meets the necessary conditions to prevent pathological fracture. The specimen staining and sectioning showed that the liver and heart of rats implanted with magnesium alloys had no pathological changes and the cell structure was normal, similar to that of rats without a magnesium alloy. Therefore, Rolled-Mg-RE alloy has good healing potential as a biodegradable implant material.

Chapter 6 Conclusions

In this study, four new magnesium alloys with different parameters were prepared by vertical two-roll continuous casting machine (VTRC), and the microstructure characteristics were analyzed by scanning Electron microscopy (SEM) and Electron backscatter diffraction (EBSD), and Mg-RE alloy was implanted into rat femur. The corrosion and bone reaction of Mg-RE alloy in vivo and the effect of long-term implantation on circulation in rats were evaluated. Understanding the corrosion behavior of magnesium alloy under different casting and implantation methods and the effects of long-term implantation on organisms is of great significance for expanding the application of magnesium based biomedical implants. The following conclusions can be drawn from the results of the experimental study:

1. The microstructure, corrosion behavior and bone reaction in vivo of Mg-RE alloy prepared by VTRC method with four casting speeds, and the effect of long-term fixation on systemic circulation were discussed. Through systematic analysis, the following conclusions are drawn:

(1) According to the microstructure of Mg-RE alloy with casting speeds of 10m/min, 16m/min, 24m/min and 30m/min was studied in detail. The results show that with the increase of casting speed, the grain size of cast-rolled pieces is finer, the amorphous integration is higher, and the corrosion resistance of the alloy increases with the increase of casting speed. Among the four Mg-RE alloys, the corrosion resistance of the Mg-RE alloy with VTRC-30m/min is the best.

(2) The results of animal experiments showed that the VTRC-30m/min group could produce more bone tissue than the VTRC-10m/min group.

(3) The staining of rat heart, liver and kidney specimens showed that the corrosion reaction of VTRC-30m/min Mg-RE alloy did not cause abnormal cell morphology, and the damage of rat liver in VTRC-10m/min group was more serious with the increase of implantation time.

(4) Serum test results showed that the serum of rats in the VTRC-30m/min group was basically the same as that in the control group, while the AST and ALT contents in the VTRC-10m/min group were higher than those in the control group during the whole experiment, indicating that the liver might be damaged. Long-term implantation of VTRC-30m/min Mg-RE alloy will not damage the body's circulation and immune system, and it is not harmful to human body.

2. According to the microstructure, corrosion behavior, and in vivo bone reaction of Rolled-Mg-RE alloys prepared by VTRC and hot rolling, as well as the effect of long-term fixation on systemic circulation, were discussed. Through systematic analysis, the following conclusions are drawn:

(1) Rolled-Mg-RE has less local orientation error and higher corrosion resistance than Mg-RE.

(2) Rolled-Mg-RE creates more bone tissue than Mg-RE.

(3) An in vivo implant degradation test showed that the degradation layer presented a two-layer structure.

(4) Staining of the rat heart and liver samples showed that the corrosion reaction of the Mg alloy plates did not cause an abnormal cell morphology.

(5) The serum biochemical test results of the Mg alloy groups were consistent with that of the control group, except for higher concentrations of Mg ions and creatinine. The

long-term implantation of the Mg alloys will not harm the circulation or immune system of the organism, indicating no harm to humans.

It's important to note that there are limitations to the study. First of all, although the serum metabolic parameters in the animal during the degradation of the implant were detected, the concentration of aluminum ion and rare earth ion in the body was not detected due to the limited detection technology, so it cannot be completely confirmed that the cause of liver injury was magnesium ion. Secondly, the expected effect of this study is that the Mg-RE alloy material is almost completely degraded, but only the amorphous phase is left and contained in the new bone. Its function is to prevent the release of Al in the alloy, thus eliminating the harm of Al to the organism. However, due to the operation duration of 48 weeks in this study, the expected ideal effect has not yet appeared. Therefore, whether Mg-RE can be completely degraded to achieve the expected effect still needs further experimental research. In addition, the mechanism of new bone formation induced by Mg-rare earth alloy remains unclear and needs further study.

References

1. International standard ISO 10993-1. Biological evaluation of medical devices-Part 1: Evaluation and testing; 2003. p. 1-12.
2. Milo?ev I. Metallic materials for biomedical applications: Laboratory and clinical studies. Pure Appl Chem. 2010; 83(2): 309-324.
3. Helsen JA, Breme HJ. Metal as biomaterials. New York: John Wily and Sons Ltd; 1998. .
4. Pickford MA, Scamp T, Harrison DH. Morbidity after gold weight insertion into the upper eyelid in facial palsy. Br J Plast Surg. 1992; 45(6): 460-464.
5. The picture is from the Internet <https://www.indiamart.com/proddetail/orthopedic-bone-plate-19799513630.html>
6. Wagoner Johnson AJ, Herschler BA. A review of the mechanical behavior of CaP and CaP/polymer composites for applications in bone replacement and repair. Acta Biomater. 2011; 7(1): 16-30.
7. Witte F, Hort N, Vogt C, Cohen S, Kainer KU, Willumeit R, et al. Degradable biomaterials based on magnesium corrosion. Curr Opin Solid St M. 2008; 12: 63-72.
8. Riaz U, Shabib I, Haider W. The current trends of Mg alloys in biomedical applications-A review. J Biomed Mater Res B Appl Biomater. 2019; 107(6): 1970-1996.
9. Liu H, D.unn ZS, Tsanhani A, Tian Q, Rodriguez A, Rivera-Castaneda L, et al. Scientific Reports 2019; 9: 1-27.

10. Wang J, Tang J, Zhang P, Li Y, Wang J, Lai Y, et al. Surface modification of magnesium alloys developed for bioabsorbable orthopedic implants: A general review. J Biomed Mater Res B Appl Biomater. 2012; 100(6): 1691-1701.
11. Tian P, Liu X. Surface modification of biodegradable magnesium and its alloys for biomedical applications. Regen Biomater. 2015; 2(2): 135-151.
12. Kumar K, Gill RS, Batra U. Challenges and opportunities for biodegradable magnesium alloy implants. Mater Technol. 2018; 33: 153-172.
13. Chen C, Karshalev E, Guan J, Wang J. Magnesium-based micromotors: water-powered propulsion, multifunctionality, and biomedical and environmental applications. Small. 2018; 14(23): e1704252.
14. Yang Y, He C, E. Dianyu, Yang W, Qi F, Xie D, et al. Mg bone implant: Features, developments and perspectives. Mater Design 2019; 185: 108259.
15. Thomann UI, Uggowitzer PJ. Wear-corrosion Behavior of Biocompatible Austenitic Stainless Steels. Wear 2000; 293(1): 48-58.
16. Devine TM, Wulff J. Cast vs wrought Cobalt-Chromium surgical implant alloys. J Biomed Mater Res. 1975; 9: 151-167.
17. Chan FW, Bobyn JD, Medley JB, Krygier JJ, Yue S, Tanzer M. Engineering issues and wear performance of metal on metal hip implants. Clin Orthop Relat Res. 1996; (333): 96-107.
18. Bothe RT, Beaton LE, Davenport HA. Reaction of bone to multiple metallic implants. Surg Gynecol Obstet. 1940; 71: 598-602.

19. Leventhal GS. Titanium, a metal for surgery. J Bone Joint Surg Am. 1951; 33(2): 473-474.

20. Staiger MP, Pietak AM, Huadmai J, Dias G. Magnesium and its alloys as orthopedic biomaterials: a review. Biomaterials 2006; 27(9): 1728-1734.

21. Liu C, Wan P, Tan LL, Wang KH, Yang K. Preclinical investigation of an innovative magnesium-based bone graft substitute for potential orthopaedic applications. J Orthop Trans. 2014; 2(3): 139-148.

22. Xie XW, Huang J, Li N, Xu W, Hu B. Progress of magnesium ions and magnesium alloy implant application in the clinical orthopaedics. Chin J Tiss Eng Res. 2012; 16(39): 7317-7321.

23. Gu XN, Zheng YF, Cheng Y, Zhong SP, Xi TF. In vitro corrosion and biocompatibility of binary magnesium alloys. Biomaterials 2009; 30(4): 484-498.

24. Gao JC, Qiao LY, Li LC, Wang Y. Hemolysis effect and calciumphosphate precipitation of heat- organic- film treated magnesium. Trans Nonferrous Met Soc China 2006; 16(3): 539-544.

25. Li LC, Gao JC, Wang Y. Evaluation of cyto-toxicity and corrosion behavior of alkali-heat-treated magnesium in simulated body fluid. Surf Coat Technol. 2004; 185: 92-98.

26. Zheng YF, Gu XN, Witte F. Biodegradable metals. Mater Sci Eng R Rep. 2014; 77: 1-34.

27. Witte F, Kaese V, Haferkamp H, Switzer E, Meyer-Lindenberg A, Wirth CJ, et al. In vivo corrosion of four magnesium alloys and the associated bone response. Biomaterials 2005; 26(17): 3557-3563.

28. Kamrani S, Fleck C. Biodegradable magnesium alloys as temporary orthopaedic implants: A review. Biometals 2019; 32(2): 185-193.

29. Shuai C, Li S, Peng S, Feng P, Lai Y, Gao C. Biodegradable metallic bone implants. Mater Chem Front. 2019; 3: 544-562.

30. Brail G, Pebere N. The corrosion of pure magnesium in aerated and desecrated sodium sulphatesolutions. Corros Sci. 2001; 43(3): 471-484.

31. Gu XN, Xie XH, Li N, Zheng YF, Qin L. In vitro and in vivo studies on a Mg-Sr binary alloy system developed as a new kind of biodegradable metal. Acta Biomater. 2012; 8(6): 2360-2374.

32. Brar HS, Wong J, Manuel MV. Investigation of the mechanical and degradation properties of Mg-Sr and Mg-Zn-Sr alloys for use as potential biodegradable implant materials. J Mech Behav Biomed Mater. 2012; 7: 87-95.

33. Huan ZG, Leeflang MA, Zhou J, Fratila Apachitei, LE, Duszczyk J. In vitro degradation behavior and cytocompatibility of Mg-Zn-Zr alloys. J Mater Sci Mater Med. 2010; 21(9): 2623-2635.

34. Zhang BP, Hou YL, Wang XD, Wang Y, Geng L. Mechanical properties, degradation performance and cytotoxicity of Mg-Zn-Ca biomedical alloys with different compositions. Mat Sci Eng C-Mater. 2011; 31(8): 1667-1173.

35. Xu ZG, Smith C, Chen S, Sankar J. Development and microstructural characterizations of Mg-Zn-Ca alloys for biomedical applications. Mat Sci Eng B 2011; 176(20): 1660-1665.

36. Hort N, Huang Y, Fechner D, St?rmer M, Blawert C, Witte F, et al. Magnesium alloys as implant materials--principles of property design for Mg-RE alloys. Acta Biomater. 2010; 6(5): 1714-1725.

37. Li YC, Wen CE, Mushahary D, Sravanthi R, Harishankar N, Pande G, et al. Mg-Zr-Sr alloys as biodegradable implant materials. Acta Biomater. 2012; 8(8): 3177-3188.

38. Hermawan H, Dubé D, Mantovani D. Developments in metallic biodegradable stents. Acta Biomater. 2010; 6(5): 1693-1697.

39. Ascencio M, Pekguleryuz M, Omanovic S. An investigation of the corrosion mechanisms of WE43 Mg alloy in a modified simulated body fluid solution: The influence of immersion time. Corros Sci. 2014; 87: 489-503.

40. Li W. Preparation technology and properties of biodegradable rare-earth magnesium alloy stent seamless tubes [Master's Thesis]. Chongqing: Chongqing University; 2011.

41. Yang JX, Cui FZ, Yin QS, Zhang Y, Zhang T, Wang XM. Characterization and degradation study of calcium phosphate coating on magnesium alloy bone implant in vitro. IEEE Trans Plasma Sci. 2009; 37: 1161-1168.

42. Yazdimamaghani M, Razavi M, Vashaee D, Tayebi L. Development and degradation behavior of magnesium scaffolds coated with polycaprolactone for bone tissue engineering. Mater. Lett. 2014; 132: 106-110.

43. Jiang W, Tian Q, Vuong T, Shashaty M, Gopez C, Sanders T, et al. Comparison study on four biodegradable polymer coatings for controlling magnesium degradation and human endothelial cell adhesion and spreading. ACS Biomater Sci Eng. 2017; 3: 936-950.

44. Lock J, Liu H. Nanomaterials enhance osteogenic differentiation of human mesenchymal stem cells similar to a short peptide of BMP-7. Int J Nanomed. 2011; 6: 2769-2777.

45. Kim SY, Kim YK, Kim KS, Lee KB, Lee MH. Enhancement of bone formation on LBL-coated Mg alloy depending on the different concentration of BMP-2. Colloid Surface B 2019; 173: 437-446.

46. Duygulu O, Kaya RA, Oktay G, Kaya AA. Investigation on the potential of magnesium alloy AZ31 as a bone implant. Mater Sci Forum 2007; 546-549: 421-424.

47. Zhang E, He W, Du H, Yang K. Microstructure, mechanical properties and corrosion properties of Mg-Zn-Y alloys with low Zn content. Mater Sci Eng A 2008; 488((12): 102-111.

48. Peng Q, Huang Y, Zhou L, Hort N, Kainer KU. Preparation and properties of high purity Mg-Y biomaterials. Biomalerials 2010; 31(3): 398-403.

49. Green AL, Ma E. Bulk Metallic glasses: At the cutting edge of metals research. MRS Bull. 2007; 32: 611-619.

50. Chen QZ, Thouas GA. Metallic implant biomaterials. Mater Sci. R 2015; 87: 1-57.

51. Wise DL, Trantolo DJ, Altobelli DE, Yaszemsk MJ, Grasser JD. Human biomaterials application. Totowa, NJ: Humana Press; 1996.

52. Yaszemsk MJ, Trantolo DJ, Lewandrowski KU, Hasirci V, Altobelli DE, Wise DL. Biomaterials in orthopedics. New York, NY: Marcel Dekker Inc; 2004.

53. Andreas AK, J?rg FL, Florian HDT. Rapid solidification and bulk metallic glasses-processing and properties. Materials processing handbook. Boca Raton, FL: CRC Press; 2007. p. 1711-1744.

54. Masumoto T, Maddin R. The mechanical properties of palladium 20 a/o silicon alloy quenched from the liquid state. Acta Metall. 1971; 19: 725-741.

55. Liebermann H, Graham C. Production of amorphous alloy ribbons and effects of apparatus parameters on ribbon dimensions. IEEE Trans Magn. 1976; 12: 921-923.

56. Narasimhan MC. Continuous casting method for metallic strips. United States Patent 4142571; 1979.

57. Inoue A, Nakamura T, Sugita T, Zhang T, Masumoto T. Bulky La-Al-TM (TM=Transition Metal) amorphous alloys with high tensile strength produced by a high-pressure die casting method. Mater Trans JIM 1993; 34: 351-358.

58. Chen HS, Miller CE. A rapid quenching technique for the preparation of thin uniform films of amorphous solids. Rev Sci Instrum. 1970; 41: 1237-1238.

59. East DR, Kellam M, Gibson MA, Seeber A, Liang D, Nie JF. Amorphous magnesium sheet produced by twin roll casting. Mater Sci Forum 2010; 654: 1078-1081.

60. Lee JG, Park SS, Lee SB, Chung HT, Kim NJ. Sheet fabrication of bulk amorphous alloys by twin-roll strip casting. Scr Mater. 2005; 53: 693-697.

61. Oh YS, Lee H, Lee J.G, Kim NJ. Twin-roll strip casting of iron-base amorphous alloys. Mater Trans. 2007; 48: 1584-1588.

62. Urata A, Nishiyama N, Amiya K, Inoue A. Continuous casting of thick Fe-base glassy plates by twin-roller melt-spinning. Mater Sci Eng A 2007; 449: 269-272.

63. Suzuki T, Anthony AM. Rapid quenching on the binary systems of high temperature oxides. Mater Res Bull. 1974; 9: 745-753.

64. Lee JG, Lee H, Oh YS, Lee S, Kim NJ. Continuous fabrication of bulk amorphous alloy sheets by twin-roll strip casting. Intermetallics 2006; 14: 987-993.

65. Hofmann DC, Roberts SN, Johnson WL. Twin roll sheet casting of bulk metallic glasses and composites in an inert environment. United States Patent Application 20130025746; 2013.

66. Ding PD, Pan FS, Jiang B, Wang J, Li HL, Wu JC, et al. Twin-roll strip casting of magnesium alloys in China. Trans Nonferrous Metals Soc China 2008; 18: s7-s11.

67. Hu X, Ju D, Zhao H. Thermal flow simulation of twin-roll casting magnesium alloy. J Shanghai Jiaotong Univ. 2012; 17: 479-483.

68. Luo LT, Gong XB, Li JZ, Kang SB, Cho JH. Microstructure and mechanical properties of severely deformed Mg-4.5Al-1.0Zn alloy processed by asymmetric rolling on ingot and twin roll cast strip. Mater Res. 2016; 19: 207-214.

69. Park SS, Park WJ, Kim CH, You BS, Kim NJ. The twin-roll casting of magnesium alloys. JOM 2009; 61: 14-18.

70. Pei ZP, Ju DY, Li X. Simulation of critical cooling rate and process conditions for metallic glasses in vertical type twin-roll casting. Trans Nonferrous Met Soc China 2017; 27: 2406-2414.

71. Liu CM, Zhu XR, Zhou HT. Magnesium alloy phase diagram. 2nd ed. Changsha: Central South University Press; 2006.

72. Wang HJ, Ju DY, Wang HW. Preparation and characterization of Mg-RE alloy sheets and formation of amorphous/crystalline composites by twin roll casting for biomedical implant application. Metals 2019; 9(10): 1075.

73. Suryanarayana C, Froes FH. Mechanical, chemical, and electrical applications of rapidly solidified alloys. In: Liebermann HH, editor. Rapidly Solidified Alloys. Boca Raton, FL: CRC Press; 1993, p. 18.

74. Wang HJ, Wang HW, Kumazawa T, Ju D, Cao J. Effect of casting speed on microstructure, corrosion behaviour and in vivo bone reaction of Mg-rare earth alloys. Sci China Technol Sc. 2021; 64(2): 213-222.

75. Holzwarth, U.; Gibson, N. The Scherrer equation versus the 'Debye-Scherrer equation'. Nat. Nanotechnol. 2011, 6, 534.

76. Pecharsky, V.K.; Zavalij, P.Y. Properties, Sources, and Detection of Radiation. Fundamentals of Powder Diffraction and Structural Characterization of Materials; Springer: Boston, MA, USA. 2009; pp. 107-132.

77. Takeuchi, A.; Inoue, A. Calculations of mixing enthalpy and mismatch entropy for ternary amorphous alloy. Mater. Trans. JIM 2000, 41, 1372-1378.

78. Inoue, A. Stabilization of metallic supercooled liquid and bulk amorphous alloys. Acta Mater. 2000, 48, 279-306.

79. Wang WH, Wu HL, Sun Y, Yan, J, Zhang L, Zhang SX, et al. Local intragranular misorientation accelerates corrosion in biodegradable Mg. Acta Biomater. 2020; 101: 575-585.

80. Wolf FI, Cittadini A. Magnesium in cell proliferation and differentiation. Front Biosci-Landmrk. 1999; 4(4): 607-617.

81. Krause A, von der H?h N, Bormann D, Krause C, Bach F-W, Windhagen H, et al. Degradation behaviour and mechanical properties of magnesium implants in rabbit tibiae. J Mater Sci Mater Med. 2010; 45(3): 624-632.

82. H?nzi AC, Gerber I, Schinhammer M, L?ffler JF, Uggowitzer PJ. On the in vitro and in vivo degradation performance and biological response of new biodegradable Mg-Y-Zn alloys. Acta Biomater. 2010; 6(5): 1824-1833.

83. Vormann J. Magnesium: nutrition and metabolism. Mol Aspects Med. 2003; 24(1-3): 27-37.

84. Yamasaki Y, Yoshida Y, Okazaki M, Shimazu A, Uchida T, Kubo T, et al. Synthesis of functionally graded MgCO3 apatite accelerating osteoblast adhesion. J Biomed Mater Res. 2002; 62(1): 99-105.

85. Xin RL, Luo YM, Zuo AL, Gao JC, Liu Q. Texture e?ect on corrosion behavior of AZ31 Mg alloy in simulated physiological environment. Mater Lett. 2012; 72: 1-4.

86. Zhang SX, Zhang XN, Zhao CL, Li JA, Song Y, Xie CY, et al. Research on an Mg-Zn alloy as a degradable biomaterial. Acta Biomater. 2010; 6: 626-640.

87. Vojtěch D, Kubásek J, Serák J, Novák P. Mechanical and corrosion properties of newly developed biodegradable Zn-based alloys for bone ?xation. Acta Biomater. 2011; 7: 3515-3522.

88. Gui Z, Kang Z, Li Y. Mechanical and corrosion properties of Mg-Gd-Zn-Zr-Mn biodegradable alloy by hot extrusion. J Alloys Compd. 2016; 685: 222-230.

89. Wang H, Kumazawa T, Zhang Y, Wang H, & Ju D. In vivo degradation behaviour and bone response of a new Mg-rare earth alloy immobilized in a rat femoral model. Mater Today Commun. 2021; 26: 101727.

90. Randall ERJR, Cohen MD, Spray JRCC, & Rossmeisl EC. Hypermagnesemia in renal failure: Etiology and toxic manifestations. Ann Intern Med. 1964; 61(1): 73-88.

91. Kontani M, Hara A, Ohta S, & Ikeda T. Hypermagnesemia induced by massive cathartic ingestion in an elderly woman without pre-existing renal dysfunction. Internal Med. 2005; 44(5): 448-452.

92. Van Hook JW. Endocrine crises. Hypermagnesemia. Crit Care Clin. 1991; 7(1): 215-223.

93. Cholst IN, Steinberg SF, Tropper PJ, Fox HE, Segre GV, & Bilezikian JP. The influence of hypermagnesemia on serum calcium and parathyroid hormone levels in human subjects. New Engl J Med. 1984; 310(19): 1221-1225.

94. Corbi G, Acanfora D, Iannuzzi G L, Longobardi G, Cacciatore F, Furgi G, et al. Hypermagnesemia predicts mortality in elderly with congestive heart disease: Relationship with laxative and antacid use. Rejuv Res. 2008; 11(1): 129-138.

95. Serre CM, Papillard M, Chavassieux P, Voegel JC, Boivin G. In?uence of magnesium substitution on a collagen-apatite biomaterial on the production of a calcifying matrix by human osteoblasts. J Biomed Mater Res. 1998; 42(4): 626-633.

96. Chakraborty Banerjee P, Al-Saadi S, Choudhary L, Harandi SE, & Singh R. Magnesium implants: Prospects and challenges. Materials, 2019; 12(1): 136.

97. Greenwald AS, Boden SD, Goldberg VM, Khan Y. Bone-graft substitutes: Facts, fictions, and applications. J Bone Joint Surg. 2001; 83(S2): S98-S103.

98. Gao JC, Qiao LY, Li LC, Wang Y. Hemolysis effect and calciumphosphate precipitation of heat- organic- film treated magnesium. T Nonferr Metal Soc Chin. 2006; 16(3): 539-544.

99. Troitskii VV, Tsitrin DN. The resorbing metallic alloy ' Osteosinthezit' as material for fastening broken bone. Khirurgiia 1944; 8(1): 41-44.

100. Cho K, Sano T, Doherty K, Yen C, Gazonas G, Montgomery J, et al. Magnesium technology and manufacturing for ultra lightweight armored ground vehicles. DTIC Document, 2009.

101. Jiang MG, Xu C, Nakata T, Yan T, Chen RS, Kamado S. Rare earth texture and improved ductility in a Mg-Zn-Gd alloy after high-speed extrusion. Mater Sci Eng A 2016; 667: 233-239.

102. Hidalgo-Manrique P, Robson JD, Pérez-Prado MT. Precipitation strengthening and reversed yield stress asymmetry in Mg alloys containing rare-earth elements: A quantitative study. Acta Mater. 2017; 124: 456-467.

103. Bhattacharyya JJ, Wang F, Wu PD, Whittington ER, El Kadiri H, Agnew SR. Demonstration of alloying, thermal activation, and latent hardening effects on quasi-static and dynamic polycrystal plasticity of Mg alloy. WE43-T5, plate. Int J Plast. 2016; 81: 123-151.

104. Castellani C, Lindtner RA, Hausbrandt P, Tschegg E, Stanzl-Tschegg SE, Zanoni G, et al. Bone-implant interface strength and osseointegration: Biodegradable magnesium alloy versus standard titanium control. Acta Biomater 2011; 7(1): 432-440.

105. Gavras S, Zhu SM, Nie JF, Gibson MA, Easton MA. On the microstructural factors affecting creep resistance of die-cast Mg-La-rare earth (Nd, Y or Gd) alloys. Mater Sci Eng A 2016; 675: 65-75.

106. Li QA, Li X, Zhang Q, Chen J. Effect of rare-earth element Sm on the corrosion behavior of Mg-6Al-1.2Y-0.9Nd alloy. Rare Metals 2010; 29(6): 557-560.

107. Pu Z, Song ZL, Yang S, Outeiro JC, Dillon OW, Puleo DA, et al. Grain refined and basal textured surface produced by burnishing for improved corrosion performance of AZ31B Mg alloy. Corros Sci. 2012; 57: 192-201.

108. Gollapudi S. Grain size distribution effects on the corrosion behaviour of materials. Corros Sci. 2012; 62: 90-94.

109. Birbilis N, Ralston KD, Virtanen S, Fraser HL, Davies CHJ. Grain character in?uences on corrosion of ECAPed pure magnesium. Corros Eng Sci Technol. 2013; 45(3): 224-230.

110. Song YW, Han EH, Shan DY, Yim CD, You BS. The role of second phases in the corrosion behavior of Mg-5 Zn alloy. Corros Sci. 2012; 60(1): 238-245.

111. Song YW, Han EH, Dong KH, Shan DY, Yim CD, You BS. Study of the corrosion product films formed on the surface of Mg-xZn alloys in NaCl solution. Corros Sci. 2014; 88: 215-225.

112. Li JR, Jiang QT, Sun HY, Li YT. Effect of heat treatment on corrosion behavior of AZ63 magnesium alloy in 3.5 wt.% sodium chloride solution. Corros Sci. 2016; 111: 288-301.

113. Wang BJ, Xu DK, Dong JH, Ke W. Effect of texture on biodegradable behavior of an as-extruded Mg-3%Al-1%Zn alloy in phosphate buffer saline medium. J Mater Sci Technol. 2016; 32(7): 646-652.

114. Song G-L. The effect of texture on the corrosion behavior of AZ31 Mg alloy. JOM 2012; 64(6): 671-679. doi:10.1007/s11837-012-0341-1

115. Wang BJ, Xu DK, Dong JH, Ke W. Effect of the crystallographic orientation and twinning on the corrosion resistance of an as-extruded Mg-3Al-1Zn (wt.%) bar. Scr Mater. 2014; 88: 5-8.

116. Pawar S, Slater TJA, Burnett TL, Zhou X, Scamans GM, Fan Z, et al. Crystallographic effects on the corrosion of twin roll cast AZ31 Mg alloy sheet. Acta Mater. 2017; 133: 90-99.

117. Zheng Y, Li Y, Chen JH, Zou ZY. Effects of tensile and compressive deformation on corrosion behaviour of a Mg-Zn alloy. Corros Sci. 2015; 90: 445-450.

118. Hu J, Shi YN, Sauvge X, Sha G, Lu K. Grain boundary stability governs hardening and softening in extremely fine nanograined metals. Science 2017; 355: 1292-1296.

119. Valiev RZ. Nanostructuring of metals by severe plastic deformation for advanced properties. Nat Mater. 2004; 3: 511-516.

120. Wang H, Ju D, Wang H. Preparation and characterization of Mg-RE alloy sheets and formation of amorphous/crystalline composites by twin roll casting for biomedical implant application. Metals 2019; 9(10): 1075.

121. Duygulu O, Kaya RA, Oktay G, Kaya AA. Investigation on the potential of magnesium alloy AZ31 as a bone implant. Mater Sci Forum 2007; 546-549: 421-424.

122. Witte F, Hort N, Vogt C, Cohen S, Feyerabend F. Degradable biomaterials based on magnesium corrosion. Curr Opin Solid State Mater Sci. 2008; 12(5): 63-72.

123. Witte F, Ulrich H, Palm C, Willbold E. Biodegradable magnesium scaffolds: Part II: peri-implant bone remodeling. J Biomed Mater Res Part A 2007; 81(3): 757-765.

124. Yang JX, Cui FZ, Lee IS, Zhang Y, Yin QS, Xia H, et al. In vivo biocompatibility and degradation behavior of Mg alloy coated by calcium phosphate in a rabbit model. J Biomater Appl. 2012; 27(2): 153-164.

125. Serre CM, Papillard M, Chavassieux P, Voegel JC, Boivin G. In?uence of magnesium substitution on a collagen-apatite biomaterial on the production of a calcifying matrix by human osteoblasts. J Biomed Mater Res. 1998; 42(4): 626-633.

126. Zhang S, Zhang X, Zhao C, Li J, Song Y, Xie C, et al. Research on an Mg-Zn alloy as a degradable biomaterial. Acta Biomater. 2010; 6(2): 626-640.

127. Bakhsheshi‐Rad HR, Idris MH, Abdul-Kadir MR, Ourdjini A, Medraj M, Daroonparvar M, et al. Mechanical and bio-corrosion properties of quaternary

Mg-Ca-Mn-Zn alloys compared with binary Mg-Ca alloys. Mater Des. 2014; 53: 283-292.

128. Zong Y, Yuan G, Zhang X, Mao L, Niu J, Ding W. Comparison of biodegradable behaviors of AZ31 and Mg-Nd-Zn-Zr alloys in Hank's physiological solution. Mater Sci Eng B. 2012; 177(5): 395-401

129. Miao H, Zhang D, Chen C, Zhang L, Pei J, Su Y, et al. Research on Biodegradable Mg-Zn-Gd Alloys for Potential Orthopedic Implants: In Vitro and in Vivo Evaluations. ACS Biomater Sci Eng. 2019; 5(3): 1623-1634.

130. Witte F, Kaese V, Haferkamp H, Switzer E, Meyer-Lindenberg A, Wirth CJ, et al. In vivo corrosion of four magnesium alloys and the associated bone response. Biomaterials.2005;26(17):3557-3563.

131. Wang H, Wang H, Kumazawa T, Ju D, Cao J. Effect of casting speed on microstructure, corrosion behaviour and in vivo bone reaction of Mg-rare earth alloys. Sci China Technol Sci. 2021; 64(2): 213-222.

132. Wang H, Kumazawa T, Zhang Y, Wang H, Ju D. In vivo degradation behaviour and bone response of a new Mg-rare earth alloy immobilized in a rat femoral model. Mater Today Commun.2021;26:101727.

Related publications

Journal Article:

1. **Zhang Y**, Wang H, Kumazawa T, Ju D. In vivo degradation and bone reaction of long-term fixation with a magnesium alloy made by twin-roll casting in a rat femur model. Bio-Med Mater Eng. 2022; 1-13.
2. **Zhang Y**, Wang H, Kumazawa T, Ju D. Effect of medical biodegradable magnesium alloy coagulation tissue refinement on in vivo degradation and bone response in a rat femur model with long-term fixation. Bio-Med Mater Eng. (accepted)

International Conferences:

1. **Zhang Y**, Wang H, Kumazawa T, Ju D. Effect of casting speed on the microstructure of Mg-rare earth alloy. 2022 11th International Conference on Material Science and Engineering Technology (ICMSET 2022). November 27, 2022. Tokyo, Japan.

Acknowledgements

I take this opportunity to express my sincere thanks to my supervisors, Prof. Dongying Ju and Prof. Takashi Kuamzawa, for accepting me as their student and giving me the opportunity to conduct my research at the Saitama Polytechnic University. I am highly indebted to them for their support, encouragement, and guidance during my study. Without their painstaking efforts in revising and polishing my drafts, the present paper would not have been possible. They have toiled immensely and spent their valuable time reading my manuscripts and suggesting further revisions, constantly helping me to improve my shortcomings.

I specially wish to thank Prof. Satou, a warm-hearted and responsible teacher and a man full of enthusiasm for research and life. In the electron microscope experiment, he provided assistance to the experimental machine. I could not have completed the experiment without his able support. Working with him has been a learning experience, both in life and in study, which shall be beneficial all throughout my life.

I also wish to thank Prof. Niwa and Prof. Hongo for attending my presentation and providing some productive advice and timely guidance, taking time out of their busy schedules to serve on my committee.

My sincere thanks are also due to all the members of Ju laboratory for their wonderful help and cooperation over the years. Finally, I am most grateful to my family for their love, support, and encouragement in my studies and postgraduate work.

February, 2022

Ying Zhang